Dietary sulfur amino acid restriction elicits a cold-like transcriptional response in inguinal but not epididymal white adipose tissue of male mice

Philip M.M. Ruppert[1], Aylin S. Güller[1], Marcus Rosendal[1], Natasa Stanic[1], Jan-Wilhelm Kornfeld[1,2]

[1]Functional Genomics and Metabolism Unit, Department for Biochemistry and Molecular Biology, University of Southern Denmark, Odense, Denmark
[2]Novo Nordisk Foundation Center for Adipocyte Signaling, University of Southern Denmark, Odense, Denmark

Keywords: Physiology, non-shivering thermogenesis, transcriptomics, thermoregulation, amino acid metabolism, adipose tissue

Correspondence should be addressed to:
Professor Jan-Wilhelm Kornfeld, Dr. rer. nat.
Department of Molecular Biology
University of Southern Denmark
Campusvej 55
DK-5230 Odense M
Email: janwilhelmkornfeld@bmb.sdu.dk
Telephone: +45 9350 7481

Abstract

Introduction: About 1 billion people are living with obesity worldwide. GLP-1-based drugs have massively transformed care, but long-term consequences are unclear in part due to reductions in energy expenditure with ongoing use. Diet-induced thermogenesis (DIT) and cold exposure (CE) raise EE via brown adipose tissue (BAT) activation and beiging of white adipose tissue (WAT). Methionine restriction (MetR) is a candidate DIT stimulus, but its EE effect has not been benchmarked against CE, nor have their tissue-level interactions been defined.

Objective & Methods: In a 2×2 design (Control vs. MetR; room temperature, RT: 22 °C vs. CE: 4 °C for 24 h), we used male C57BL/6N mice to benchmark MetR-induced thermogenesis against CE and mapped how diet and temperature interact across tissues. Bulk RNA-seq profiled liver, iBAT, iWAT, and eWAT. Differential expression was modeled with main effects and a diet×temperature interaction. KEGG GSEA was used to assess pathway-level enrichment.

Results: MetR increased EE at RT and shifted fuel use towards lipid oxidation, supporting MetR as a bona fide DIT stimulus. CE elevated EE across diets and blunted diet differences. Transcriptomic responses were tissue-specific: in liver, CE dominated gene induction while MetR and CE cooperatively repressed genes. The combination enriched glucagon/AMPK-linked and core metabolic pathways. In iBAT, CE dominated thermogenic and lipid-oxidation programs with minimal MetR contribution. In iWAT, MetR and CE acted largely additively with high concordance, enhancing fatty-acid degradation, PPAR signaling, thermogenesis, and TCA cycle pathways. In eWAT, robust co-dependent and synergistic differential expression emerged only with MetR+CE.

Conclusion: MetR is a genuine DIT stimulus that remodels metabolism in a tissue-specific manner. Our study provides a tissue-resolved transcriptomic resource that benchmarks diet-induced (MetR) against cold-induced thermogenesis and maps their interactions across liver, iBAT, iWAT, and eWAT.

Introduction

Obesity has become a global health crisis, with prevalence rates reaching alarming levels in many countries. The World Health Organization (WHO) estimates that over 890 million adults worldwide are obese (1), leading to a dramatic increase in obesity-related diseases such as type 2 diabetes, cardiovascular disease, and certain cancers. As traditional weight-loss strategies often fail to provide lasting results, new therapeutic approaches are urgently needed. The increase in energy expenditure via brown adipose tissue (BAT) activation has emerged as a promising strategy for combating obesity. Unlike white adipose tissue (WAT), which stores excess energy, BAT is specialized in generating heat and driving energy expenditure via non-shivering-thermogenesis, typically in response to cold exposure (CE). Pharmacologically or environmentally induced BAT activity results in improved metabolic health in mice and humans (2,3). Conversely, diet-induced thermogenesis (DIT) refers to the increase in energy expenditure associated with the digestion, absorption, and metabolism of food.

Recent studies have suggested that sulfur amino acid restriction, also referred to as Methionine restriction (MetR), a dietary intervention that limits the intake of the amino acids Methionine and Cysteine, can enhance energy expenditure (EE) and promote metabolic health (4). Methionine and Cysteine are amino acids involved in a plethora of metabolic reactions including protein synthesis, gene expression via methylation of DNA and histones, maintenance of DNA and RNA integrity via polyamine synthesis, redox balance via glutathione and H_2S metabolism, and nucleotide biosynthesis via the folate cycle (4,5).

Studies have shown that MetR is sensed in the liver by the GCN2-PERK-ATF4-mediated integrated stress response (6). Initially, it was thought that increases in circulating FGF21 drive increases in EE by activating UCP1-driven thermogenesis in brown adipose tissue via β-adrenergic (βr) signaling (4,7). However, more recent studies also show that least some of the metabolic benefits develop in βr-incompetent, FGF21-KO and UCP1-KO animals, with or without increases in EE and independently of ambient temperature (5,6,8,9), highlighting the complexity of the physiological response to the dietary restriction of sulfur amino acids. Recently, it has been proposed that sulfur amino acid restriction results in metabolic inefficiency resulting in the excretion of various metabolites including β-hydroxybutyrate, pyruvate, citrate, alpha-ketoglutarate, carnosine and others (10).

Above-mentioned studies highlight an intriguing overlap between diet- and cold-induced thermogenesis, particularly in the context of energy expenditure regulation. Both stimuli rely on the activation of brown adipose tissue (BAT) and the 'beiging' of inguinal white adipose tissue (iWAT) to promote UCP1 expression and increase mitochondrial activity, and thereby boost calorie dissipation, potentially via similar signaling pathways, including the sympathetic nervous system and key metabolic regulators like FGF21 (11). However, whether diet- and cold-induced thermogenesis produce additive or synergistic effects on the activation of energy and systemic metabolism is unknown. Here, we systematically compare the physiological and transcriptional responses to MetR and CE across multiple metabolically active tissues. Using RNA-sequencing, we dissect additive, synergistic, and antagonistic gene regulatory patterns, and assess whether combining MetR with CE produces tissue-specific concordant or discordant novel transcriptional outcomes.

We demonstrate that MetR increased EE at RT and shifted fuel use toward lipid oxidation. CE elevated EE across diets and blunted diet differences. The transcriptional responses were tissue-specific on gene and pathway level. Taken together, our results provide a unique and comprehensive gene regulatory framework to understand how dietary and environmental cues converge to shape tissue-specific gene expression programs and metabolic adaptation.

Materials & Methods:

All animal experiments were performed in accordance with the Directive 2010/63/EU from the European Union and approved by the Ministry of Environment and Agriculture Denmark (Miljø- og Fødevarestyrelsen) under license no. 2018-15-0201-01544.

Animal husbandry & experiments

All experiments were performed in male mice on a C57Bl/6N background (Taconic, Denmark). All mice were housed under a 12-hour light/dark cycle in a temperature and humidity-controlled facility and had ad libitum access to diets and drinking water. 8/9-week-old were acclimatized to our animal facility on a chow diet (NIH-31, Zeigler Brothers Inc., 8% calories from fat) and housed in groups of 3-4 animals per cage for the habituation period. For reproducibility reasons and to avoid biases by 'social thermogenesis' we single-housed all mice for the duration of the experiments and concluded the experiments with mice being 16 weeks of age.

In study 1 we performed indirect calorimetry to assess physiological effects and interactions between diets and ambient temperature. For this 15 mice were split randomly into 3 groups and fed cysteine-depleted diets containing either 0.8% Methionine (Control; Ctrl), 0.12% Methionine (Methionine-restricted; MetR) or 2% Methionine (Methionine-supplemented; MetS) for 6 days at 22ºC and 5 days at 4ºC. Diets were from Research diets (New Brunswick, NJ, USA). Exact compositions can be retrieved under cat.no. A11051301B (MetR), A11051302B (Ctrl) and A21060801 (MetS).

In study 2, we performed detailed analyses of physiological (body and organ weights) and molecular parameters (RNA-seq, colorimetric/enzymatic assays) to investigate the molecular adaptations and interactions between diet and temperature. For this 28 mice were split randomly into 4 groups and were either fed previously mentioned Ctrl or MetR diets at 22ºC for 7 days or housed an additional 8th day at 4 ºC. Blood glucose were determined just prior to sacrifice in the cage using a standard glucometer . The mice were then euthanized by carbon dioxide asphyxiation followed by cervical dislocation. Blood was collected by cardiac puncture and stored on ice for the duration of the sacrifice. Serum was collected after centrifugation by 2,000 g for 15 min and stored at -80 °C. Mice were sacrificed by carbon dioxide euthanasia. Liver, eWAT, iWAT and BAT were weighed and snap-frozen in liquid nitrogen and then stored at -80 °C.

Indirect calorimetry

Indirect calorimetry was conducted using the PhenoMaster NG 2.0 Home Cage System (TSE systems, Bad Homburg, Germany). Prior to the experiment, a complete calibration protocol for the gasanalysers was run according to the manufacturer's recommendations, and the mice were weighed. Mice were housed individually and acclimated to the new environment for 3 days prior to the experiment. The machine was set to maintain 50% humidity throughout the experiment and a 12-hour light/dark cycle, with ad libitum access to food and water. During the experiment energy expenditure, respiratory exchange ratio, food and water intake were recorded every 60 seconds and datapoints were filtered for outliers and then averaged per hour for the analysis. Indirect calorimetry data are presented as mean ± SEM.

RNA sequencing and analysis

Total RNAs from tissues were isolated using the TRI reagent (Sigma) followed by clean-up with RPE buffer (Qiagen, Germany). The quality of RNA was validated by the Agilent RNA 6000 Nano-Kit in Agilent 2100 Bioanalyzer according to the manufacturer's protocol (Agilent Technologies, Waldbronn, Germany). mRNA sequencing was performed in-house. After quality control 500 ng RNA in a final volume of 25 µL DEPC-treated water was prepared and sample preparation was performed as described in the NEBNext Poly(A) mRNA Magnetic Isolation Module kit and NEBNext Ultra II RNA Library Prep Kit (cat no: #E7770, New England Biolabs, Ipswich, MA, USA). The amplified libraries were validated by Agilent 2100 Bioanalyzer using a DNA 1000 kit (Agilent Technologies, Inc., Santa Clara, CA, USA) and quantified by qPCR using the KaPa Library Kits (KaPa Biosystems, Wilmington, MA, USA). Hereafter, 2x50bp paired-end sequencing was performed on Illumina Novaseq 6000.

RNAseq data analysis

Sequencing reads were aligned to the mouse reference genome (Gencode vM25) (12) using STAR aligner (v2.7.9a) (13) with the following parameters: --outSAMunmapped Within, --outFilterType BySJout, --outSAMattributes NH HI AS NM MD, --outFilterMultimapNmax 10, --outFilterMismatchNoverReadLmax 0.04, --alignIntronMin 20, --alignIntronMax 1000000, --alignMatesGapMax 1000000, --alignSJoverhangMin 8, and --alignSJDBoverhangMin 1. Gene-level quantification was performed using featureCounts (v2.0.3) (14). In parallel, transcript-level quantification was performed using Salmon (v1.9.0) (15) and Gencode vM25, with parameters --seqBias, --useVBOpt, and --numBootstraps 30. Transcript abundance estimates were imported and summarized to the gene level using the

tximport package (16). Quality control was summarized with MultiQC v1.19. All RNA-seq samples passed the QC. Differential gene expression analysis was performed using DESeq2 (v1.46.0) (17) with shrinkage of fold-changes using apeglm (18). Genes with fewer than 10 total counts across all samples were excluded prior to normalization. The following interaction model was applied: ~ diet + temperature + diet:temperature, allowing detection of diet effects, temperature effects, and their statistical interaction. Specifically, the model tested: (i) the main effect of diet (MetR vs. Ctrl), (ii) the main effect of temperature (CE vs. RT), and (iii) the diet × temperature interaction (whether the effect of MetR differs between RT and CE). Genes with an adjusted p-value < 0.05 and an absolute $\log_2 FC \geq 0.585$ were considered significantly differentially expressed. Gene set enrichment analysis (GSEA) was performed using the gseKEGG() function from the clusterProfiler package (v4.14.6) (19) with parameters: organism = "mmu", pvalueCutoff = 1, pAdjustMethod = "BH", minGSSize = 0, seed = TRUE, and eps = 0. Quality control metrics and preprocessing approaches were done as previously described (20).

RNAseq outlier detection

Outlier detection was performed upon visual inspection of PCA plots within tissue analyses and was supported by robustPCA from the rrcov package (v1.7.7) (21). From the 7 samples per group and tissue, in the order of Ctrl_RT, Ctrl_CE, MetR_RT and MetR_CE the following number of samples were excluded in the transcriptomic analysis: 0, 0, 0 and 0 (Liver), 0, 1, 0 an 0 (iBAT), 0, 0, 0, and 0 (iWAT) and 3, 0, 1, and 0 (eWAT).

Classification of transcriptional interaction

Differentially expressed genes were classified according to their regulation across single and combined stimuli using a custom R script adapted from García *et al.* (22). The four relevant contrasts were defined as Ctrl_CE vs Ctrl_RT (A), MetR_RT vs Ctrl_RT (B), MetR_CE vs Ctrl_RT (AB), and the interaction term (A×B). Only genes significant (padj < 0.05 and $|FC| > 1.5$) in at least one comparison were included. For each gene, the direction of regulation (Up, Down, Unchanged) was assigned for every contrast. Genes were then first classified as cooperative when both single exposures (A and B) changed in the same direction or remained unchanged, or as competitive when they differed (e.g., one Up, one Down, or only one significant). Based on these combinations, genes were grouped into distinct regulation categories: co-dependent (significant only in AB but not in A or B), concordant (both A and

B regulated in the same direction and AB responded similarly), discordant (A and B regulated in the same direction but AB changed oppositely), Ctrl_CE- or MetR_RT-dominant (competitive single exposures where AB followed A or B), and masked (Fig. 3D). Masked genes were defined as significant in one or both single exposures but not in AB: Ctrl_CE-masked (significant only in A), MetR_RT-masked (significant only in B), or mutually masked (significant in both A and B but lost in AB, indicating opposing regulation under the combined stimulus) (Fig. S3C). To evaluate synergy, an expected additive effect was computed as the sum of log□ fold changes from the single exposures (expected{A+B} = log□FC{A} + log□FC{B}). The synergy score was calculated as log□ of the absolute ratio between the observed combined effect (log□FC{AB}) and the expected additive effect, i.e., log□|log□FC{AB}/expected{A+B}|. When this expected additive effect was approximately zero, synergy was considered undefined for that gene. Genes without significant interaction effects were classified as "additive." Genes with significant interaction effects were further assigned as "synergistic" (synergy score > 0) or "antagonistic" (synergy score < 0), reflecting whether the observed combined effect surpassed or fell short of additivity. The regulation patterns are exemplified in Fig. 3D and Fig. S3C.

Data availability

The RNA-seq data generated in this study have been deposited in the NCBI Gene Expression Omnibus (GEO) under accession number GSEXXXXXX. The dataset includes raw FASTQ files, processed count matrices, and metadata for all experimental conditions. In addition lists of all DEGs and GSEA analysis from each tissue were provided in the supplementary files.

Serum measurements

Serum NEFA's were determined using the NEFA-HR(2) kit (cat. no. 434-91795 and 436-91995; FUJIFILM Wako Chemicals Europe GmbH). Serum triglycerides were determined using the LabAssay Triglyceride kit (cat no. 291-94501; FUJIFILM Wako Chemicals Europe GmbH). Serum β-hydroxybutyrate levels were determined using the β-HBA kit (cat. no. 2940; Instruchemie, Delfzijl, the Netherlands). Serum FGF21 and IL-6 levels were determined using the Luminex Multiplex platform (R&D Systems).

Statistics

Statistical analysis of the transcriptomics data was performed as described in the previous paragraph. Serum, body and organ weight data were analyzed using GraphPad Prism (v. 10.4.1). Prior to the analysis, the assumptions of normality and homogeneity of variance were assessed. These assumptions were met in all presented parameters. Plasma parameters, absolute and relative organ weights and bodyweight change (%) were analyzed using an unpaired one-way ANOVA with Tukey's HSD test to correct for multiple comparisons. Statistical differences between the groups were depicted in a compact letter display, were groups with the same letter are not significantly different and groups with different letters are significantly different. Bodyweight data (start/finished) and average daily locomotor activity and food and water intake (RT/CE) were analyzed using a paired two-way ANOVA with Tukey's HSD test to correct for multiple comparisons. Statistical differences between the groups were depicted as * $p < 0.05$, ** $p < 0.01$, *** $p < 0.001$, **** $p < 0.0001$. Energy expenditure, food and water intake data from the indirect calorimetry experiment was analyzed by ANCOVA with bodyweight or locomotor activity as covariate. The ANCOVA analysis was done pairwise using the regression tool at by NIDDK Mouse Metabolic Phenotyping Centers (MMPC, www.mmpc.org).

Results

Physiological and metabolic effects of methionine restriction (MetR) and cold exposure (CE)

To investigate the physiological impact of dietary sulfur amino acid content on EE under room temperature (RT, i.e., 22°C) and cold exposure (CE, 4°C for 24h), male C57BL/6N mice were placed one of three cysteine-depleted diets containing either 0.8% Methionine (Control; Ctrl), 0.12% Methionine (Methionine-restricted; MetR) or 2% Methionine (Methionine-supplemented; MetS) for six and five days, respectively (Fig. 1A, i.e. study 1). Following the diet switch from housing diet to aforementioned experimental diets, EE increased progressively in the MetR group under RT conditions, rising from approx. 0.45 kcal/h to 0.6 kcal/h. Conversely, EE did not change in the Ctrl and MetS groups (Fig. 1B). On day six, energy expenditure in the MetR group was significantly elevated compared to Ctrl and MetS groups, independent of starting bodyweight (Fig. 1C, left). In contrast, CE elevated EE in all 3 diet groups to ~ 0.9 kcal/h, thereby rescinding the differences between MetR and the other two diets at RT (Fig. 1A, 1C right, Fig. S1A). MetR-fed animals exhibited significantly greater body weight loss compared to Ctrl and MetS-fed animals over the total duration of experimental diet feeding (Fig. 1D). As food intake and locomotor activity were similar across groups (Fig. S1B, S1D), the greater weight loss in MetR-fed animals is likely attributable to increased energy expenditure under RT conditions.

Consistent with previous studies, MetR feeding also increased water intake (Fig. S1C). Respiratory exchange ratios (RER), as an indicator for macronutrient fuel selection, progressively increased during light and dark phases in the Ctrl and MetS groups, indicating enhanced carbohydrate utilization, whereas MetR-fed animals demonstrated lower RER indices, indicating a preference for lipid oxidation. Upon CE, RER decreased in Ctrl and MetS-fed animals to levels comparable to those observed in MetR-fed animals (Fig. 1E, S1F). To further assess dietary and temperature interactions, we calculated daily averages of food and water intake, as well as locomotor activity and RER for each period. At RT, daily caloric intake was similar between groups and CE led to a consistent increase in caloric intake in all groups (Fig. 1F). Average daily water intake was unaffected by ambient temperature, whereas daily locomotor activity exhibited a downward trend in all three groups during cold exposure (Fig. 1F, Fig. S1E). Collectively, these data demonstrate that short-term MetR increases energy expenditure by ca. 20% at RT and, as a consequence, promotes a metabolic shift toward lipid oxidation, potentially due to a transcriptional induction of thermogenic processes and/or lipolysis in catabolic adipose tissue depots such as iWAT or

BAT. However, CE as major physiological stimulus to induce non-shivering thermogenesis (NST) was able to override this MetR-induced effect, prompting an additional ca. 60% increase in EE independent of experimental diet feeding and body weight, alongside a shift to lipid utilization.

To further investigate the potential interactions between MetR- and CE-induced thermogenesis on physiological, metabolic and transcriptional parameters a second experiment was conducted: Here, mice were divided into four groups and either fed Ctrl or MetR diets (see study 1) for seven days at 22°C, or additionally exposed to 4°C for 24h (Study 2). In the following, animals fed Ctrl or MetR diets for 7 days at 22°C are denominated as Ctrl_RT and MetR_RT, while animals fed these diets for 7 days before being subjected to 24h of cold are denominated as Ctrl_CE and MetR_CE (Fig. 1G). All groups experienced significant body weight loss during the intervention (Fig. 1H), presumably due to single-housing. Counterintuitively, Ctrl_CE did not display exacerbated weight loss compared to the Ctrl_RT group. By contrast, MetR_RT led to approximately 10% body weight loss, and the combinational treatment (MetR_CE) resulted in further weight loss compared to MetR_RT alone (Fig. 1H). The reductions in body weights coincided with organ-specific alterations in organ wet weights and organ/bodyweight ratios. Both Ctrl_CE and MetR_RT resulted in absolute (Fig. 1I) and relative (Fig. S1G) reductions in liver mass and MetR_CE reduced absolute and relative liver mass further in an additive fashion. The stepwise reduction in relative liver mass indicates that liver atrophy partly accounted for the observed body weight loss, predominantly in MetR-exposed mice. In contrast, Ctrl_CE alone did not affect iWAT, gWAT, or iBAT mass. Intriguingly, under MetR_RT all three adipose tissues showed (non-significant) upward trends in relative and absolute masses, which was exacerbated and partially significant under MetR_CE (Fig. 1I, Fig. S1G). Intriguingly, these data indicate that MetR_RT and Ctrl_CE synergize to promote increases adipose tissue mass particularly in gWAT and iBAT. To assess the associated systemic metabolic sequelæ of MetR- and CE , we measured circulating metabolic parameters: Blood glucose levels did not change significantly, but displayed a stepwise reduction between the groups, indicating additive effects between diet and ambient temperature (Fig. 1J). In line with previous studies, serum triglyceride where reduced, albeit non-significantly, by Ctrl_CE and MetR_RT (23–25), but showed an even stronger reduction under MetR_CE, suggesting synergy (Fig. 1J). By contrast, serum NEFA levels showed only minor non-significant reductions in both CE conditions and were unchanged by MetR_RT alone (Fig. 1J), while serum β-hydroxybutyrate levels, a marker of hepatic fatty acid oxidation, was elevated by either CE or MetR feeding

(Fig. S1H). A major hormonal stimulus of EE in response to CE or MetR is mediated via 'thermogenic' hormones like FGF21 or IL-6. In line with the literature, Ctrl_CE and MetR_RT elevated circulating FGF21 levels even though the effect of cold was limited in this study. FGF21 levels did not further increase under MetR_CE, indicating that MetR maximally activates *Fgf21* transcription / FGF21 secretion to induce EE (Fig. 1J). In contrast to literature, Ctrl_CE resulted in significant reductions in serum IL-6 levels in this study (Fig. S1H) (26). MetR_RT also reduced serum IL-6 levels, with no further alterations under MetR_CE (Fig. S1H). Together, these results suggest that while Cold exposure and MetR feeding individually trigger overlapping metabolic responses, their combination produces additive effects on weight loss, liver atrophy, and adipose size, alongside specific synergistic effects on triglyceride levels.

The transcriptional responses to CE and MetR-induced thermogenesis are tissue-specific

To investigate the transcriptional basis of the adaptation to two independent, yet potentially synergistic, physiological stimulators of NST, we next performed bulk mRNA-seq on liver, iBAT, iWAT, and eWAT across all four groups. Principal Component Analysis (PCA), as expected, revealed that the samples clustered according to their tissue of origin (Fig. S2A). We next performed tissue-intrinsic PCA analyses that demonstrated highly tissue-specific responses (Fig. 2A). (1) In the Liver, all 4 groups showed distinct transcriptional responses in PC1 and PC2 whereas in (2) iBAT the groups clustered mostly by temperature (PC1), indicating that the transcriptional effects of MetR feeding are mild compared to CE. By contrast in both white adipose depots the 4 groups showed significant overlap although, in (3) iWAT, the clusters showed additive effects of MetR and CE along PC1, explaining 60% of the variation, while in (4) eWAT the clusters overlapped in PC1 and PC2. Differential gene expression analysis (cutoff: adj. pvalue < 0.05, $|FC| \geq 1.5$) showed that Ctrl_CE elicited stronger responses than MetR_RT in all tissues as exemplified by the higher number of differentially expressed genes (DEGs) without clear trends towards global transcriptional induction or repression. Of note, MetR was coupled to a higher number of repressed genes, potentially linked to the increased need for cellular energy conservation during amino acid-restriction. The combination of both stimuli elicited the strongest transcriptional responses in iWAT and apart from the interaction term, the transcriptional response in eWAT appeared limited (Fig. 2B, S2B).

To understand to what degree the transcriptional responses are tissue / depot-specific or broadly applicable to all investigated organs, we analyzed the intersections between CE and

MetR in all four tissues (Fig. 2C-F, S2C, D). Under Ctrl_CE and MetR_CE more than 50% of all DEG's were regulated in a tissue-specific manner in 3 out of the 4 tissues, with the most marked transcriptional effects seen in iWAT (Fig. 2C-E). The degree of tissue-specific regulation was even higher in MetR_RT and in the interaction term (Fig. 2D,F). Cumulatively, these data suggest that the majority of transcriptional effects of CE and dietary MetR are tissue-specific and display a varying degree of additive and synergistic effects.

To better scrutinize the individual transcriptional effects for each tissue, and to associate the observed gene-regulatory effects with cellular and metabolic processes, we next performed binary, combinatorial analyses of differential gene expression in liver (Fig. 3), iBAT (Fig. 4), iWAT (Fig. 5) and eWAT (Fig. 6) using similar in silico approaches.

CE drives gene induction while MetR and CE cooperatively repress genes in the liver

In the liver (Fig. 3), Volcano plot analysis revealed substantial gene regulation induced by Ctrl_CE (977 genes upregulated, 322 genes downregulated) and MetR_RT (257 genes upregulated, 387 genes downregulated), with even more genes regulated when combined under MetR_CE (815 genes upregulated, 692 genes downregulated). While Ctrl_CE appears to be a stronger stimulus based on the number of DEGs, MetR_RT appears to elicit stronger transcriptional effects based on log□FC (Fig. 3A). Based on the number of DEGs, MetR_RT and Ctrl_CE, when combined under MetR_CE, appear to repress gene expression in an independent, additive manner and induce genes in a dependent or antagonistic manner (Fig. 3A). Indeed only a very limited number of genes were significant in diet × temperature interaction term (36 genes upregulated, 77 genes downregulated; Fig. 3A) and the transcriptional effects of CE under MetR (MetR_CE vs MetR_RT) and MetR feeding under CE (MetR_CE vs Ctrl_CE) were lower compared to their respective counterparts (Fig. S3A). To gain further insights into the degree of overlap between Ctrl_CE and MetR_RT, we performed Upset plot analysis. The biggest set of shared genes was found between Ctrl_CE and MetR_CE (541 DEGs), highlighting that Ctrl_CE is a major contributor to the transcriptional effects seen in MetR_CE (Fig. 3B). While the direct of contribution of MetR_RT alone was lower (251 DEGs), this analysis also indicated a high degree of co-dependence on MetR_RT in the regulation of 508 DEGs in the MetR_CE condition, as well as the exclusion of 494 Ctrl_CE DEGs from the combined exposure (Fig. 3B). Contrasting all MetR_CE DEGs between Ctrl_CE and MetR_RT (R^2 = 0.34), as well as contrasting all MetR_RT and Ctrl_CE DEGs (R^2 = 0.26) revealed relatively poor correlation between the respective log□FC values and suggests that the overall influence of Cold is stronger (Fig. 3C,

Fig. S3B). Next we analyzed the transcriptional interaction between Ctrl_CE and MetR_RT (Fig. 3D, S3C, see methods) under consideration of significance, direction of regulation and interaction significance based on the method proposed by García *et al.* (22). This analysis indicated that more than 50% of down-regulated genes were due to co-dependent additive regulation between Ctrl_CE and MetR_RT (brown) and MetR_RT alone (green). By contrast, more than 50% of the up-regulated genes were significant in the combined exposure due to Ctrl_CE alone (Fig. 3D). Altogether, these data confirm Ctrl_CE drives the induction of genes under MetR_CE, while Ctrl_CE and MetR_RT cooperate to repress genes under MetR_CE. On the other hand, MetR_RT prevented a significant number of Ctrl_CE DEGs (n = 547 genes) from regulation under MetR_CE an additive (subtractive) fashion (Fig. S3D). Finally, to understand which pathways are differentially regulated, we performed Gene set enrichment analysis (GSEA) under consideration of log□FC values (27). Among the 20 most enriched pathways under MetR_CE, MetR drove the enrichment for metabolic pathways (Biosynthesis of amino acids, Glutathione or P450 cytochrome (Drug) metabolism) despite the effects of Ctrl_CE, while CE drove the enrichment in Steroid biosynthesis and cGMP-PKG signaling pathways, despite the effects of MetR_RT (Fig. 3F). These results are in line with previously published datasets (28,29). This analysis also revealed a number of gene sets where MetR_CE showed the highest enrichment, such as Glucagon and AMPK signaling, TCA cycle, One carbon metabolism and amino acid biosynthesis. This indicates that MetR and CE cooperate in the regulation of gene sets related to energy provisioning and glucose metabolism in the liver (Fig. 3F). The top 30 heatmap of induced genes under MetR_CE reflects these additive effects of Ctrl_CE and MetR_RT on the level of pathway enrichment and features genes such as *Pck2* and *Lepr* (Glucagon signaling), *Pck2* (TCA cycle), *Mthfd1l* and *Aldh1l2* (TCA cycle and folate metabolism), and *Psat1*, *Etnppl* and *Acot4* (amino acid biosynthesis) (Fig. 3G). The only non-immune related pathway among the 14 most negatively enriched pathways was the Ribosome gene set, where Cold and MetR feeding had opposing effects (Fig. 3H). In accordance with the contrasting enrichment by MetR_RT and Ctrl_CE alone, the top 30 heatmap of MetR_CE repressed genes only features immune-related genes including *Saa1*, *Saa2*, *Saa3* and *Orm1* and *Orm2* (acute-phase response), *Lcn2* and *Lrg1* (innate immunity) (Fig. 3I). Furthermore, additional heatmap analyses of the top 30 up- and down-regulated genes for Ctrl_CE and MetR_RT further highlight the distinct and cooperative transcriptional effects between both stimuli (Fig. S3E-J).

CE dominates gene induction in iBAT with limited contribution by MetR feeding

In iBAT (Fig. 4), Volcano plot analysis revealed that Ctrl_CE elicited a much stronger transcriptional response than MetR_RT (757 genes upregulated, 912 genes downregulated, versus 57 genes upregulated and 173 downregulated, respectively). The transcriptional response to MetR_CE was only marginally different from Ctrl_CE (664 genes upregulated, 1091 genes downregulated), suggesting that the majority of the transcriptional response is driven by CE (Fig. 4A). Only a very small number of genes were identified in the diet × temperature interaction term (22 upregulated, 21 downregulated), indicating that the combination of CE and MetR does not result in non-additive transcriptional effects in iBAT (Fig. 4A). In line with this, CE on top of MetR (MetR_CE vs MetR_RT) still resulted in substantial gene regulation (Fig. S4A). Upset plot analysis confirmed that the majority of DEGs in the combined MetR_CE condition overlapped with Ctrl_CE (1009 genes), while only a minor subset was shared with MetR_RT (85 genes; Fig. 4B). Comparison of log□FC between Ctrl_CE and MetR_RT for all MetR_CE DEGs showed a weak correlation (R^2 = 0.24), supporting the notion that the transcriptional responses to MetR_CE are indeed driven by CE (Fig. 4C). This weak correlation was confirmed when considering all MetR_RT or Ctrl_CE DEGs (Fig. S4B). The classification of gene-regulation confirmed that >50% of down- and up-regulated genes were driven by Ctrl_CE (blue, Fig. 4D). Altogether, these data indicate that Ctrl_CE primarily drives gene regulation in iBAT, while the transcriptional effects of MetR_RT are negligible. GSEA analysis confirmed the positive enrichment of fatty acid and thermogenic pathways by Ctrl_CE, as previously published (29,30). The combination of both stimuli specifically benefited the positive enrichment of metabolic pathways such as Fatty acid elongation, Biosynthesis of unsaturated fatty acids and PPAR signaling, while Ctrl_CE drove the enrichment in ER and glycerolipid related gene sets. In line with the limited transcriptional response of MetR_RT on gene level, NES scores for MetR_RT were mostly lower compared to Ctrl_CE and/or non-significant, except for Steriod biosynthesis (Fig. 4E). In line, the heatmap of the top 30 upregulated genes under MetR_CE underscores this enrichment by featuring important factors such as *Ppargc1a*, *Fgf21*, *Gdf15*, *Gpr3* and *Bmp8b* (PPAR signaling and thermogenesis), *Elovl3* and *Scd3* (fatty acid elongation), and *Mthfd2* (folate metabolism) (Fig. 4F). Many of these genes are also featured in the top 30 heatmap for Ctrl_CE regulated genes (Fig. S4D). By contrast, negatively enriched gene sets under MetR_CE were largely immune- and extracellular matrix–related, including, cytokine-, ECM- and neuroactive ligand- receptor interactions and cell adhesion gene sets (*Col1a1*, *Col1a2*, *Ngfr*, *Hcar2*, *Adcy5*). Interestingly, the negative enrichment of these pathways was dominated by MetR_RT (Fig. 4G,H). Altogether, these analysis support

the notion that the transcriptional effects of MetR_RT are limited and contribute little to the combined effect of MetR_CE, which is dominated by cold (Fig. S4D-G).

Additive and synergistic gene regulation by MetR and CE in iWAT

In iWAT (Fig. 5), Volcano plots revealed that both Ctrl_CE (992 upregulated, 1379 genes downregulated) and MetR_RT (680 upregulated, 1156 downregulated) elicited marked transcriptional changes: The combination of both stimuli (MetR_CE) resulted in an even greater number of DEGs compared to either stimuli alone (1394 upregulated, 2261 downregulated), indicating either additive or synergistic effects (Fig. 5A). Only a limited number of genes were identified in the diet × temperature interaction (188 down, 55 up), suggesting few non-additive responses (Fig. 5A). Upset plots suggest cooperativity between MetR_RT and Ctrl_CE, with 1234 DEGs uniquely regulated when both stimuli were combined, but also support true additive or synergistic regulation with 1210 genes being significantly regulated in all three conditions (Fig. 5B). Correlation of log□FC between Ctrl_CE and MetR_RT for all MetR_CE showed a strong positive correlation ($R^2 = 0.81$), suggesting that the impact of CE and MetR feeding on gene regulation is similar in iWAT (Fig. 5C, S5B). Regulatory classification of MetR_CE DEGs revealed that 55% of up- and 75% of down-regulated genes were predominantly regulated in an additive manner, where Ctrl_CE and MetR_RT cooperated to enhance transcriptional responses. This included genes that became significant when both stimuli were combined (co-dependent regulation) as well as genes that were already significantly regulated under each condition alone but showed non-synergistic regulation under the combined treatment (concordant – additive; Fig. 5D). GSEA analysis revealed in pathways consistent with expected CE- or MetR-induced responses, such as fatty acid degradation, PPAR signaling, thermogenesis, and the TCA cycle (Fig. 5E) (29,30). Notably, nearly all of these pathways showed significant negative enrichment for the interaction term, indicating that the transcriptional response to MetR_CE is less than additive. This suggests that while both Ctrl_CE and MetR_RT independently activate key metabolic pathways, their combined effect is attenuated on the gene set level, possibly due to overlapping mechanisms or transcriptional feedback limiting further activation. Heatmap analysis of the top 30 induced genes matches GSEA results and features prominent PPAR and thermogenesis related genes including *Dio2, Ucp1, Fgf21, Elovl3, Cpt1b* and *Ppargc1a*. The heatmap analysis also confirms the largely additive gene regulatory effects of Ctrl_CE and MetR_RT on gene level (Fig. 5F, S5D,E). Similar to the responses in iBAT, also iWAT showed negative enrichment in predominantly immune-

related pathways, such as cytokine-cytokine receptor interactions (*Ccl2, Ccl7, Ccl8, Ccl12, Ccr5, Il1rl1*) (Fig. 5G,H).

Limited yet codependent and antagonistic gene regulation by MetR and CE in eWAT

In eWAT (Fig. 6), Volcano plot analysis revealed that both CE and MetR feeding alone did not have substantial effects on transcription, as less than 189 DEGs were up- or down-regulated in either condition (Fig. 6A). This combined effect under MetR_CE also featured merely 122 up- or down-regulated genes, while the interaction term identified 193 up- and 292 down-regulated DEGs, the highest among all tissues, suggesting a potential synergistic mode of gene regulation under MetR_CE in this tissue (Fig. 6A). Upset plot analysis confirmed that most MetR_CE DEGs (158) are unique to the combination of CE and MetR, and that Ctrl_CE (31 DEGs) or MetR_RT (24 DEGs) alone contributed little to the joined MetR_CE effect (Fig. 6B). Scatter plot analysis of log□FC values between Ctrl_CE and MetR_RT for all MetR_CE DEGs revealed a relatively high correlation ($R^2 = 0.54$) and were predominantly categorized as Co-dependent–additive (brown) (Fig. 6C, D). Conversely, all DEGs from either Ctrl_CE or MetR_RT correlated less with each other ($R^2 = 0.29$), and were found to interact in an antagonistic fashion (Fig. S6B,C). This suggests a complex gene-regulatory relationship between MetR feeding and CE in eWAT. On the one hand, MetR_RT and Ctrl_CE additively regulate genes that only become significant under MetR_CE, on the other hand DEGs unique to MetR_RT or Ctrl_CE alone are excluded from the combined MetR_CE response in an antagonistic fashion. GSEA analysis revealed that significant positive enrichment in immune and signaling pathways such as Rap1 signaling, MAPK signaling, and cGMP-PKG signaling (*Maff*, *Ptchd4*, and *Arhgef37*) under the combined treatment of MetR_CE (Fig. 6E,F). Here interaction between MetR_RT and Ctrl_CE enrichment scores appeared additive in nature (non-signicant enrichment for interaction DEGs). Intriguingly, negatively enriched pathways under MetR_CE were largely associated with fatty acid metabolism and oxidative phosphorylation (Fig. 6G). While, MetR_RT alone again did not result in significant enrichment here, Ctrl_CE often resulted in opposing (significant or non-significant) enrichment for the mentioned pathways. These enrichments match with repressed genes that are regulated in an additive manner between MetR_RT and Ctrl_CE (*Cyp2e1, Cyp4f17, Ehhadh, Slc16a1, Serpina3b*; Fig. 6H) and genes that are regulated in an antagonistic manner (*Acly, Elovl6, Angptl8, Acss2, Me1, Fasn, Scd2, Acaca,*

Slc25a1; Fig. S6F,I). Overall, these results highlight a complex relationship between both thermogenic stimuli in eWAT comprising both additive but also antagonistic regulation on gene and pathway level.

Discussion

In this work, we compared the systemic effects of two environmental stimuli of energy expenditure, dietary MetR and CE, in a 2x2 design, in order to assess whether both stimuli produce additive or synergistic systemic energy metabolism and transcriptional adaptations in key metabolic tissues. Our results indicate that although dietary MetR increased EE at RT and shifted substrate utilization towards lipid oxidation, CE constituted a stronger stimulus for EE and masked diet-dependent differences. Combining CE and MetR resulted in mild reductions in bodyweight and glucose levels and additive reductions on circulating triglyceride levels and liver mass. Notwithstanding the threshold effects seen in the activation of FGF21 and β-hydroxybutyrate (βOHB), markers for energy homeostasis and hepatic fatty acid oxidation, respectively, these results suggest that there is potential incombining both stimuli for the correction of hyperglycemia, hypertriglyceridemia and excess bodyweight in disease settings.

To gain further insights into how MetR and CE converge on the transcriptional level we performed RNA-seq on liver, iBAT, iWAT and eWAT. We observed a high degree of depot-specificity in the transcriptional responses to MetR, CE and the combination, both on gene and pathway level. In liver, CE dominated gene induction while MetR and CE cooperatively repressed genes. The combination of both factors regulated pathways involved in energy and glucose handling (Glucagon signaling, TCA cycle, AMPK signaling, Amino acid & Carbon metabolism), potentially explaining the stepwise reduction in circulating glucose and triglyceride levels. In iBAT, CE dominated the transcriptional response, with limited contribution from MetR, and resulted in the enrichment of thermogenic and lipid-oxidation programs (thermogenesis, fatty acid metabolism). In iWAT, MetR and CE acted largely additively with high concordance, enhancing fatty-acid degradation, PPAR signaling, thermogenesis, and TCA cycle pathways. The transcriptional responses in eWAT overall were limited, producing some additional, yet mostly antagonistic effects. Whether the downregulation of fatty acid metabolism pathways is linked to the relative increase of eWAT mass under MetR_CE requires further investigation.

An intriguing finding of potential translational value was the cold-like transcriptional response elicited by MetR feeding in iWAT. Amidst the emerging appreciation that the amount and metabolic activity of ‘classical’ human brown adipocytes might not contribute to overall EE and metabolic regulation in humans (31), other fat depots such as ‘beige’

subcutaneous adipose tissue (scWAT, i.e., the functional human equivalent to murine iWAT) are moving into the limelight of fundamental research and therapeutic pursuits (32). This is spurred by the appreciation that human, just like rodent, white fat exerts important catabolic and endocrine functions (33), begetting the seminal question about the nature of physiological, pharmacological, dietary and lifestyle-associated interventions that will help achieve to increase energy dissipation via scWAT. Here, the unsolved task is to prompt uncoupling protein 1 (UCP1)-dependent and UCP1-independent biochemical processes such as Ca^{2+}/creatine cycling (34,35), or by inducing an energy-consuming combination of triacylglycerol breakdown and fatty acid re-esterification that occurs after sympathomimetic administration (36) selectively in beige fat. Intriguingly, a recent report demonstrated that oral supplementation of high-fat diet fed mice with a nitroalkene derivative of salicylate (SANA) can induce creatine cycling in rodent iWAT independent of UCP1, demonstrating that the activation of iWAT thermogenesis and mitochondrial respiration is exploitable using pharmacology. Noteworthy, a Phase 1 study demonstrated that human volunteers receiving SANA exhibited a modest degree of weight loss, suggesting that strategies for iWAT mobilization in rodents might translate to (obese) patients (37). To date, orthogonal nutritional approaches for iWAT activation in mice rely on negative energy balances and include calorie restriction paradigms such as intermittent fasting (38), yet conclusive data on their effect in human scWAT remains limited (39,40) and might incur detrimental processes such as the unwanted mobilization of lean (muscle and bone) mass. The selective omission or removal of methionine and cysteine have proven to be efficient in activating EE via iWAT thermogenesis, and involve both humoral (FGF21 secretion) and sympathetic nervous system-dependent, UCP1-independent responses (9,9,10,29). Future studies with extended durations should clarify whether run-in dietary priming, e.g. via dietary MetR, can enhance adaptive thermogenic responses during prolonged cold exposure, ideally monitored by continuous measurement of core body temperature and more in-depth molecular analysis of the browning phenotype in iWAT.

An intriguing opportunity for dietary MetR might lie in maximizing treatment effects against more clinical conditions ranging from cancer (41,42) to obesity. Here, drugs that mimic the action of the gut hormone glucagon-like peptide-1 (GLP1), i.e., so called GLP1 receptor agonists (GLP1Ra) such as semaglutide, have radically transformed obesity treatment and reduce body weight via reducing appetite (43). However, to date these drugs have the unfortunate downside of unfavorably reducing EE (44). As lead-in calorie restriction allows

mice to maintain EE and thus enhance the degree of achievable weight loss (45), nutritional approaches might help to break the efficacy plateau that continue to plague GLP1Ras, collectively highlighting the notion that dietary interventions such as selective amino acid restriction prior or during pharmacological treatment deserve further experimental exploration and clinical testing.

Classically, DIT is synonymous with the thermic effect of food (TEF) and describes the post-prandial rise in energy expenditure attributable to digestion, absorption, and metabolic processing of nutrients (46). This canonical, meal-linked DIT is transient and scales with meal energy composition (47). In contrast, dietary MetR elevates EE independent of acute feeding by engaging an endocrine-neuronal axis, where hepatic amino-acid sensing activates the integrated stress response, increases FGF21 expression and circulating levels, and drives thermogenesis in WAT/BAT and a state of metabolic inefficiency, thereby increasing EE (4,5,10). Related protein-restriction paradigms similarly raise EE through FGF21-mediated thermogenic programs (48). Our and previous data demonstrate that MetR increases EE at thermoneutral-adjacent conditions and elicits depot-specific thermogenic transcriptional programs, even when benchmarked against cold exposure. We propose that MetR represents a true form of “diet-induced thermogenesis” in a mechanistic sense i.e., a diet composition-initiated, hormone-driven thermogenic state that is distinct from the classic meal-processing TEF.

Altogether, our study provides important initial insights into depot-specific transcriptional responses to MetR, CE, and their combination, yet several limitations remain. The relatively short duration (7 days MetR, 24-hour CE) was sufficient for assessing acute transcriptional interactions but limited our ability to investigate long-term physiological adaptations or sustained metabolic remodeling. Furthermore, applying complementary omics analyses, including proteomics and metabolomics or flux analysis would provide deeper mechanistic insights into metabolic interactions at the protein and metabolite levels.

Acknowledgements

We thank all the members of the Kornfeld lab for fruitful discussions. We gratefully acknowledge the assistance of the FGM-seq team for their help with the sequencing measurements and Victor Goitea for helpful discussions around outlier detection methods of RNA-seq samples. All of the computation done for this project was performed on the UCloud interactive HPC system, which is managed by the eScience Center at the University of Southern Denmark. This work was supported by an EMBO Long-Term Fellowship (ALTF 676-2021) to PMMR and a Novo Nordisk Foundation call NNF21OC0070263 to PMMR and JWK.

Author Contributions

P.M.M.R.: Conceptualization; Methodology; Validation; Formal analysis; Investigation; Visualization; Supervision; Project administration; Funding acquisition; Writing – original draft; Writing – review & editing.

M.R.: Investigation.

A.S.G.: Investigation.

N.S.: Investigation.

JW.K.: Conceptualization; Resources; Validation; Formal analysis; Supervision; Project administration; Funding acquisition; Writing – review & editing.

Conflict of Interest Statement

The authors declare that they have no conflict of interest.

Figure legends:

Figure 1. Physiological and metabolic effects of methionine restriction (MetR) and cold exposure (CE). (A) Schematic depicting 11 day experimental setup and dietary composition for mouse experiment 1 (n = 5 animals/group). (B) Energy expenditure (EE) over the entire experiment duration. (C) ANCOVA analysis of average nighttime EE on days 6 and 11 over body weight. (D) Bodyweight and body weight loss (%). (E) Respiratory exchange ratio (RER) over the entire experiment duration. (F) Average daily food and water intake over all RT (22 °C) or CE (4 °C) experimental days. (G) Schematic depicting 8 day experimental setup for mouse experiment 2 (n = 7 animals/group). Dietary compositions for Ctrl and MetR diets are the same as in mouse experiment 1. Groups are denominated as Ctrl_RT, Ctrl_CE, MetR_RT and MetR_CE. (H) Bodyweight and body weight loss (%). (I) Absolute organ weights for Liver, inguinal WAT, gonadal WAT, interscapular BAT. Statistics were done within tissues. (J) Blood glucose, serum triglycerides, and FGF21 levels. EE was analyzed by ANCOVA using body weight as a covariate (via mmpc.org); p-values were Bonferroni-corrected. Bodyweight, average food and water intake were analyzed via two-way ANOVA with *p□<□0.05, **p□<□0.01, ***p□<□0.001, ****p□<□0.0001. Body Weight loss, serum parameters and absolute organ weights were analyzed using one-way ANOVA with Tukey's post hoc test. Different letters indicate statistically significant differences (p□<□0.05). Samples sizes for experiment 1 are 5 animals/group and 5-7 animals/group for Experiment 2.

Figure 2. The transcriptional responses to Cold exposure (CE) and MetR-induced thermogenesis are tissue-specific. (A) Tissue-specific PCA plots for Liver, iBAT, iWAT, and eWAT. (B) Number of differentially expressed genes (DEGs), split into induced (red) and repressed (blue) genes, per contrast (adjusted p-value < 0.05, |FC| > 1.5). (C-F) UpSet plots showing overlap of DEGs across tissues for each contrast: (C) Ctrl_CE vs Ctrl_RT, (D) MetR_RT vs Ctrl_RT, (E) MetR_CE vs Ctrl_RT, and (F) Interaction. Set size bars indicate the total number of DEGs per tissue; intersection bars indicate the number of shared DEGs between tissues. Dots and bars in orange represent tissue-specific DEGs. In the order of Ctrl_RT, Ctrl_CE, MetR_RT and MetR_CE the following number of samples were included in the transcriptomic analysis: 7, 7, 7 and 7 (Liver), 7, 6, 7 an 7 (iBAT), 7, 7, 7, and 7 (iWAT) and 4, 7 6, and 7 (eWAT) (see methods).

Figure 3. Cold exposure (CE) drives gene induction while methionine restriction (MetR) and CE cooperatively repress genes in the liver. (A) Volcano plots showing DEGs for each contrast (Ctrl_CE vs Ctrl_RT, MetR_RT vs Ctrl_RT, MetR_CE vs Ctrl_RT, and the diet × temperature interaction). Numbers indicate significantly up- and downregulated genes (adjusted p-value < 0.05, |FC| > 1.5). (B) Upset plot showing the overlap of DEGs across contrasts. Intersection bars indicate the number of shared DEGs between contrasts. Dots in orange represent contrast-specific DEGs. (C) Scatter plot of log□FC values in Ctrl_CE vs Ctrl_RT and MetR_RT vs Ctrl_RT for DEGs identified in MetR_CE. n denominates DEGs shown. (D) Schematic highlighting gene expression profiles. Arrows indicate significant regulation for induced (up; red) or repressed (down; blue) genes. Non-significant regulation is depicted as grey dots (see methods). (E) Classification of MetR_CE DEGs based on their mode of regulation mode. (F) GSEA of the top 20 positively enriched pathways in MetR_CE vs Ctrl_RT. Dot size represents gene ratio, color denotes contrast, and significance is indicated by filled circles (adjusted p-value < 0.05). (G) Heatmap of Top 30 induced genes under MetR_CE. (H) GSEA for the top 14 negatively enriched pathways in the MetR_CE vs Ctrl_RT comparison. Dot size reflects gene ratio, colors indicate contrast group, and significance is shown by filled circles (adjusted p-value < 0.05). (I) Heatmap of Top 30 repressed genes under MetR_CE.

Figure 4. CE dominates gene induction in iBAT with limited contribution by MetR feeding (A) Volcano plots showing DEGs for each contrast (Ctrl_CE vs Ctrl_RT, MetR_RT vs Ctrl_RT, MetR_CE vs Ctrl_RT, and the diet × temperature interaction). Numbers indicate significantly up- and downregulated genes (adjusted p-value < 0.05, |FC| > 1.5). (B) Upset plot showing the overlap of DEGs across contrasts. Intersection bars indicate the number of shared DEGs between contrasts. Dots in orange represent contrast-specific DEGs. (C) Scatter plot of log□FC values in Ctrl_CE vs Ctrl_RT and MetR_RT vs Ctrl_RT for DEGs identified in MetR_CE. n denominates DEGs shown. (D) Classification of MetR_CE DEGs based on their mode of regulation mode. (E) GSEA of the top 10 positively enriched pathways in MetR_CE vs Ctrl_RT. Dot size represents gene ratio, color denotes contrast, and significance is indicated by filled circles (adjusted p-value < 0.05). (F) Heatmap of Top 30 induced genes under MetR_CE. (G) GSEA for the top 20 negatively enriched pathways in the MetR_CE vs

Ctrl_RT comparison. Dot size reflects gene ratio, colors indicate contrast group, and significance is shown by filled circles (adjusted p-value < 0.05). (H) Heatmap of Top 30 repressed genes under MetR_CE.

Figure 5. Additive and synergistic gene regulation by MetR and CE in iWAT (A) Volcano plots showing DEGs for each contrast (Ctrl_CE vs Ctrl_RT, MetR_RT vs Ctrl_RT, MetR_CE vs Ctrl_RT, and the diet × temperature interaction). Numbers indicate significantly up- and downregulated genes (adjusted p-value < 0.05, |FC| > 1.5). (B) Upset plot showing the overlap of DEGs across contrasts. Intersection bars indicate the number of shared DEGs between contrasts. Dots in orange represent contrast-specific DEGs. (C) Scatter plot of log□FC values in Ctrl_CE vs Ctrl_RT and MetR_RT vs Ctrl_RT for DEGs identified in MetR_CE. n denominates DEGs shown. (D) Classification of MetR_CE DEGs based on their mode of regulation mode. (E) GSEA of the top 20 positively enriched pathways in MetR_CE vs Ctrl_RT. Dot size represents gene ratio, color denotes contrast, and significance is indicated by filled circles (adjusted p-value < 0.05). (F) Heatmap of Top 30 induced genes under MetR_CE. (G) GSEA for the top 20 negatively enriched pathways in the MetR_CE vs Ctrl_RT comparison. Dot size reflects gene ratio, colors indicate contrast group, and significance is shown by filled circles (adjusted p-value < 0.05). (H) Heatmap of Top 30 repressed genes under MetR_CE.

Figure 6. ***Limited yet codependent and antagonistic gene regulation by MetR and CE in eWAT*** (A) Volcano plots showing DEGs for each contrast (Ctrl_CE vs Ctrl_RT, MetR_RT vs Ctrl_RT, MetR_CE vs Ctrl_RT, and the diet × temperature interaction). Numbers indicate significantly up- and downregulated genes (adjusted p-value < 0.05, |FC| > 1.5). (B) Upset plot showing the overlap of DEGs across contrasts. Intersection bars indicate the number of shared DEGs between contrasts. Dots in orange represent contrast-specific DEGs. (C) Scatter plot of log□FC values in Ctrl_CE vs Ctrl_RT and MetR_RT vs Ctrl_RT for DEGs identified in MetR_CE. n denominates DEGs shown. (D) Classification of MetR_CE DEGs based on their mode of regulation mode. (E) GSEA of the top 10 positively enriched pathways in MetR_CE vs Ctrl_RT. Dot size represents gene ratio, color denotes contrast, and significance is indicated by filled circles (adjusted p-value < 0.05). (F) Heatmap of Top 30 induced genes under MetR_CE. (G) GSEA for the top 20 negatively enriched pathways in the MetR_CE vs

Ctrl_RT comparison. Dot size reflects gene ratio, colors indicate contrast group, and significance is shown by filled circles (adjusted p-value < 0.05). (H) Heatmap of Top 30 repressed genes under MetR_CE.

Supplementary figure legends:

Supplemental figure 1. (A) ANCOVA analysis of average nighttime EE on days 6 and 11 over average nighttime locomotor activity. (B) Cumulative food intake (kcal) over the entire study period. (C) Cumulative water intake (mL) over the entire study period. (D) Cumulative locomotor activity (beam breaks) over the entire study period. (E) Average daily locomotor activity over all RT (22 °C) or CE (4 °C) experimental days. (F) Average light and dark phase RER at days 4-6 (RT) and days 9-11 (CE). (G) Relative organ weights for liver, iWAT, gWAT, iBAT. Statistics were done within tissues. (H) Serum β-hydroxybutyrate (βOHB), Non-esterified fatty acids (NEFA) and IL-6 levels. EE was analyzed by ANCOVA using average locomotor activity as a covariate (via mmpc.org); p-values were Bonferroni-corrected. Average daily locomotor activity, and average RER were analyzed via two-way ANOVA with *p□<□0.05, **p□<□0.01, ***p□<□0.001, ****p□<□0.0001. Serum parameters and relative organ weights were analyzed using one-way ANOVA with with Tukey's post hoc test. Different letters indicate statistically significant differences (p□<□0.05). Samples sizes for experiment 1 are 5 animals/group and 5-7 animals/group for Experiment 2.

Supplemental figure 2. (A) PCA plot of all RNA-seq samples colored by tissue and shaped by experimental group. (B) Number of DEGs (adjusted p-value < 0.05, |FC| > 1.5) in each tissue across the indicated comparisons, split into up- (red) and down- (blue) regulated genes. (C-D) UpSet plots showing overlap of DEGs across tissues for each contrast: (C) MetR_CE vs MetR_RT, (D) MetR_CE vs Ctrl_CE. Set size bars indicate the total number of DEGs per tissue; intersection bars indicate the number of shared DEGs between tissues. Dots and bars in orange represent tissue-specific DEGs. In the order of Ctrl_RT, Ctrl_CE, MetR_RT and MetR_CE the following number of samples were included in the transcriptomic analysis: 7, 7, 7 and 7 (Liver), 7, 6, 7 an 7 (iBAT), 7, 7, 7, and 7 (iWAT) and 4, 7 6, and 7 (eWAT) (see methods).

Supplementary Figure 3. (A) Volcano plots showing DEGs for MetR_CE vs MetR_RT (left) and MetR_CE vs Ctrl_CE (right). Numbers indicate significantly up- and

downregulated genes (adjusted p-value < 0.05, |FC| > 1.5). (B) Scatter plot comparing log□FC values in Ctrl_CE vs Ctrl_RT and MetR_RT vs Ctrl_RT for DEGs significant in either condition. Colored dots indicate DEGs specific to each contrast or MetR_CE. n denominates DEGs shown. (C) Schematic highlighting gene expression profiles. Arrows indicate significant regulation for induced (up; red) or repressed (down; blue) genes. Non-significant regulation is depicted as grey dots (see methods). (D) Regulation classification of DEGs found in Ctrl_CE vs Ctrl_RT (left) or MetR_RT vs Ctrl_RT (right), but not MetR_CE vs Ctrl_RT. (E) Heatmap of Top 30 genes induced under Ctrl_CE. (F) Heatmap of Top 30 genes induced under MetR_RT. (G) Heatmap of Top 30 genes with negative interaction. (H) Heatmap of Top 30 genes repressed under Ctrl_CE. (I) Heatmap of Top 30 genes repressed under MetR_RT. (J) Heatmap of Top 30 genes with positive interaction.

Supplementary Figure 4. (A) Volcano plots showing DEGs for MetR_CE vs MetR_RT (left) and MetR_CE vs Ctrl_CE (right). Numbers indicate significantly up- and downregulated genes (adjusted p-value < 0.05, |FC| > 1.5). (B) Scatter plot comparing log□FC values in Ctrl_CE vs Ctrl_RT and MetR_RT vs Ctrl_RT for DEGs significant in either condition. Colored dots indicate DEGs specific to each contrast or MetR_CE. n denominates DEGs shown. (C) Regulation classification of DEGs found in Ctrl_CE vs Ctrl_RT (left) or MetR_RT vs Ctrl_RT (right), but not MetR_CE vs Ctrl_RT. (D) Heatmap of Top 30 genes induced under Ctrl_CE. (E) Heatmap of Top 30 genes induced under MetR_RT. (F) Heatmap of Top 30 genes with negative interaction. (G) Heatmap of Top 30 genes repressed under Ctrl_CE. (H) Heatmap of Top 30 genes repressed under MetR_RT. (I) Heatmap of Top 30 genes with positive interaction.

Supplementary Figure 5. (A) Volcano plots showing DEGs for MetR_CE vs MetR_RT (left) and MetR_CE vs Ctrl_CE (right). Numbers indicate significantly up- and downregulated genes (adjusted p-value < 0.05, |FC| > 1.5). (B) Scatter plot comparing log□FC values in Ctrl_CE vs Ctrl_RT and MetR_RT vs Ctrl_RT for DEGs significant in either condition. Colored dots indicate DEGs specific to each contrast or MetR_CE. n denominates DEGs shown. (C) Regulation classification of DEGs found in Ctrl_CE vs Ctrl_RT (left) or MetR_RT vs Ctrl_RT (right), but not MetR_CE vs Ctrl_RT. (D) Heatmap of Top 30 genes induced under Ctrl_CE. (E) Heatmap of Top 30 genes induced under MetR_RT. (F) Heatmap of Top 30 genes with negative interaction. (G) Heatmap of Top 30 genes repressed under Ctrl_CE. (H) Heatmap of Top 30 genes repressed under MetR_RT. (I) Heatmap of Top 30 genes with positive interaction.

Supplementary Figure 6. (A) Volcano plots showing DEGs for MetR_CE vs MetR_RT (left) and MetR_CE vs Ctrl_CE (right). Numbers indicate significantly up- and downregulated genes (adjusted p-value < 0.05, |FC| > 1.5). (B) Scatter plot comparing log□FC values in Ctrl_CE vs Ctrl_RT and MetR_RT vs Ctrl_RT for DEGs significant in either condition. Colored dots indicate DEGs specific to each contrast or MetR_CE. n denominates DEGs shown. (C) Regulation classification of DEGs found in Ctrl_CE vs Ctrl_RT (left) or MetR_RT vs Ctrl_RT (right), but not MetR_CE vs Ctrl_RT. (D) Heatmap of Top 30 genes induced under Ctrl_CE. (E) Heatmap of Top 30 genes induced under MetR_RT. (F) Heatmap of Top 30 genes with negative interaction. (G) Heatmap of Top 30 genes repressed under Ctrl_CE. (H) Heatmap of Top 30 genes repressed under MetR_RT. (I) Heatmap of Top 30 genes with positive interaction.

References

1. Phelps NH, Singleton RK, Zhou B, Heap RA, Mishra A, Bennett JE, et al. Worldwide trends in underweight and obesity from 1990 to 2022: a pooled analysis of 3663 population-representative studies with 222 million children, adolescents, and adults. The Lancet. 2024 Mar;403(10431):1027–50.

2. Schlein C, Heeren J. Implications of thermogenic adipose tissues for metabolic health. Best Pract Res Clin Endocrinol Metab. 2016 Aug;30(4):487–96.

3. Yoneshiro T, Aita S, Matsushita M, Kayahara T, Kameya T, Kawai Y, et al. Recruited brown adipose tissue as an antiobesity agent in humans. J Clin Invest. 2013 Aug;123(8):3404–8.

4. Fang H, Stone KP, Wanders D, Forney LA, Gettys TW. The Origins, Evolution, and Future of Dietary Methionine Restriction. Annu Rev Nutr. 2022 Aug 22;42:201–26.

5. Forney LA, Fang H, Sims LC, Stone KP, Vincik LY, Vick AM, et al. Dietary Methionine Restriction Signals to the Brain Through Fibroblast Growth Factor 21 to Regulate Energy Balance and Remodeling of Adipose Tissue. Obes Silver Spring Md. 2020 Oct;28(10):1912–21.

6. Wanders D, Burk DH, Cortez CC, Van NT, Stone KP, Baker M, et al. UCP1 is an essential mediator of the effects of methionine restriction on energy balance but not insulin sensitivity. FASEB J Off Publ Fed Am Soc Exp Biol. 2015 June;29(6):2603–15.

7. Babygirija R, Lamming DW. The regulation of healthspan and lifespan by dietary amino acids. Transl Med Aging. 2021;5:17–30.

8. Wanders D, Forney LA, Stone KP, Burk DH, Pierse A, Gettys TW. FGF21 Mediates the Thermogenic and Insulin-Sensitizing Effects of Dietary Methionine Restriction but Not Its Effects on Hepatic Lipid Metabolism. Diabetes. 2017 Apr;66(4):858–67.

9. Lee AH, Orliaguet L, Youm YH, Maeda R, Dlugos T, Lei Y, et al. Cysteine depletion triggers adipose tissue thermogenesis and weight loss. Nat Metab. 2025 June;7(6):1204–22.

10. Varghese A, Gusarov I, Gamallo-Lana B, Dolgonos D, Mankan Y, Shamovsky I, et al. Unravelling cysteine-deficiency-associated rapid weight loss. Nature. 2025 July 17;643(8072):776–84.

11. Spann RA, Morrison CD, den Hartigh LJ. The Nuanced Metabolic Functions of Endogenous FGF21 Depend on the Nature of the Stimulus, Tissue Source, and Experimental Model. Front Endocrinol. 2021;12:802541.

12. Mudge JM, Carbonell-Sala S, Diekhans M, Martinez JG, Hunt T, Jungreis I, et al. GENCODE 2025: reference gene annotation for human and mouse. Nucleic Acids Res. 2025 Jan 6;53(D1):D966–75.

13. Dobin A, Davis CA, Schlesinger F, Drenkow J, Zaleski C, Jha S, et al. STAR: ultrafast universal RNA-seq aligner. Bioinforma Oxf Engl. 2013 Jan 1;29(1):15–21.

14. Liao Y, Smyth GK, Shi W. featureCounts: an efficient general purpose program for assigning sequence reads to genomic features. Bioinforma Oxf Engl. 2014 Apr 1;30(7):923–30.

15. Patro R, Duggal G, Love MI, Irizarry RA, Kingsford C. Salmon provides fast and bias-aware quantification of transcript expression. Nat Methods. 2017 Apr;14(4):417–9.

16. Soneson C, Love MI, Robinson MD. Differential analyses for RNA-seq: transcript-level estimates improve gene-level inferences. F1000Research. 2015;4:1521.

17. Love MI, Huber W, Anders S. Moderated estimation of fold change and dispersion for RNA-seq data with DESeq2. Genome Biol. 2014;15(12):550.

18. Zhu A, Ibrahim JG, Love MI. Heavy-tailed prior distributions for sequence count data: removing the noise and preserving large differences. Bioinforma Oxf Engl. 2019 June 1;35(12):2084–92.

19. Yu G, Wang LG, Han Y, He QY. clusterProfiler: an R package for comparing biological themes among gene clusters. Omics J Integr Biol. 2012 May;16(5):284–7.

20. Davidsen LI, Hagberg CE, Goitea V, Lundby SM, Larsen S, Ebbesen MF, et al. Mouse vascularized adipose spheroids: an organotypic model for thermogenic adipocytes. Front Endocrinol. 2024;15:1396965.

21. Todorov V. rrcov: Scalable Robust Estimators with High Breakdown Point [Internet]. The R Foundation; 2004 [cited 2025 Oct 13]. (CRAN: Contributed Packages). Available from: https://CRAN.R-project.org/package=rrcov

22. Pantaleón García J, Kulkarni VV, Reese TC, Wali S, Wase SJ, Zhang J, et al. OBIF: an omics-based interaction framework to reveal molecular drivers of synergy. NAR Genomics Bioinforma. 2022 June;4(2):lqac028.

23. Grefhorst A, Van Den Beukel JC, Dijk W, Steenbergen J, Voortman GJ, Leeuwenburgh S, et al. Multiple effects of cold exposure on livers of male mice. J Endocrinol. 2018 Aug;238(2):91–106.

24. Hasek BE, Boudreau A, Shin J, Feng D, Hulver M, Van NT, et al. Remodeling the Integration of Lipid Metabolism Between Liver and Adipose Tissue by Dietary Methionine Restriction in Rats. Diabetes. 2013 Oct 1;62(10):3362–72.

25. Bartelt A, Bruns OT, Reimer R, Hohenberg H, Ittrich H, Peldschus K, et al. Brown adipose tissue activity controls triglyceride clearance. Nat Med. 2011 Feb;17(2):200–5.

26. Bal NC, Maurya SK, Pani S, Sethy C, Banerjee A, Das S, et al. Mild cold induced thermogenesis: are BAT and skeletal muscle synergistic partners? Biosci Rep. 2017 Oct 31;37(5):BSR20171087.

27. Subramanian A, Tamayo P, Mootha VK, Mukherjee S, Ebert BL, Gillette MA, et al. Gene set enrichment analysis: a knowledge-based approach for interpreting genome-wide expression profiles. Proc Natl Acad Sci U S A. 2005 Oct 25;102(43):15545–50.

28. Zhang Z, Cheng L, Ma J, Wang X, Zhao Y. Chronic Cold Exposure Leads to Daytime Preference in the Circadian Expression of Hepatic Metabolic Genes. Front Physiol. 2022;13:865627.

29. Ghosh S, Forney LA, Wanders D, Stone KP, Gettys TW. An integrative analysis of tissue-specific transcriptomic and metabolomic responses to short-term dietary methionine restriction in mice. PloS One. 2017;12(5):e0177513.

30. Hao Q, Yadav R, Basse AL, Petersen S, Sonne SB, Rasmussen S, et al. Transcriptome profiling of brown adipose tissue during cold exposure reveals extensive regulation of glucose metabolism. Am J Physiol Endocrinol Metab. 2015 Mar 1;308(5):E380-392.

31. Becher T, Palanisamy S, Kramer DJ, Eljalby M, Marx SJ, Wibmer AG, et al. Brown adipose tissue is associated with cardiometabolic health. Nat Med. 2021 Jan;27(1):58–65.

32. Sun W, Modica S, Dong H, Wolfrum C. Plasticity and heterogeneity of thermogenic adipose tissue. Nat Metab. 2021 June;3(6):751–61.

33. Blondin DP. Human thermogenic adipose tissue. Curr Opin Genet Dev. 2023 June;80:102054.

34. Rahbani JF, Roesler A, Hussain MF, Samborska B, Dykstra CB, Tsai L, et al. Creatine kinase B controls futile creatine cycling in thermogenic fat. Nature. 2021 Feb;590(7846):480–5.

35. Ikeda K, Kang Q, Yoneshiro T, Camporez JP, Maki H, Homma M, et al. UCP1-independent signaling involving SERCA2b-mediated calcium cycling regulates beige fat thermogenesis and systemic glucose homeostasis. Nat Med. 2017 Dec;23(12):1454–65.

36. Blondin DP, Nielsen S, Kuipers EN, Severinsen MC, Jensen VH, Miard S, et al. Human Brown Adipocyte Thermogenesis Is Driven by β2-AR Stimulation. Cell Metab. 2020 Aug 4;32(2):287-300.e7.

37. Cal K, Leyva A, Rodríguez-Duarte J, Ruiz S, Santos L, Garat MP, et al. A nitroalkene derivative of salicylate, SANA, induces creatine-dependent thermogenesis and promotes weight loss. Nat Metab. 2025 June 17;

38. Li G, Xie C, Lu S, Nichols RG, Tian Y, Li L, et al. Intermittent Fasting Promotes White Adipose Browning and Decreases Obesity by Shaping the Gut Microbiota. Cell Metab. 2017 Oct 3;26(4):672-685.e4.

39. Roth CL, Molica F, Kwak BR. Browning of White Adipose Tissue as a Therapeutic Tool in the Fight against Atherosclerosis. Metabolites. 2021 May 14;11(5):319.

40. Plummer JD, Johnson JE. Intermittent methionine restriction reduces IGF-1 levels and produces similar healthspan benefits to continuous methionine restriction. Aging Cell. 2022 June;21(6):e13629.

41. Gao X, Sanderson SM, Dai Z, Reid MA, Cooper DE, Lu M, et al. Dietary methionine influences therapy in mouse cancer models and alters human metabolism. Nature. 2019 Aug;572(7769):397–401.

42. Sanderson SM, Gao X, Dai Z, Locasale JW. Methionine metabolism in health and cancer: a nexus of diet and precision medicine. Nat Rev Cancer. 2019 Nov;19(11):625–37.

43. Müller TD, Blüher M, Tschöp MH, DiMarchi RD. Anti-obesity drug discovery: advances and challenges. Nat Rev Drug Discov. 2022 Mar;21(3):201–23.

44. Löffler MC, Betz MJ, Blondin DP, Augustin R, Sharma AK, Tseng YH, et al. Challenges in tackling energy expenditure as obesity therapy: From preclinical models to clinical application. Mol Metab. 2021 Sept;51:101237.

45. Petersen J, Merrild C, Lund J, Holm S, Clemmensen C. Lead-in calorie restriction enhances the weight-lowering efficacy of incretin hormone-based pharmacotherapies in mice. Mol Metab. 2024 Nov;89:102027.

46. Calcagno M, Kahleova H, Alwarith J, Burgess NN, Flores RA, Busta ML, et al. The Thermic Effect of Food: A Review. J Am Coll Nutr. 2019 Aug;38(6):547–51.

47. Swaminathan R, King RF, Holmfield J, Siwek RA, Baker M, Wales JK. Thermic effect of feeding carbohydrate, fat, protein and mixed meal in lean and obese subjects. Am J Clin Nutr. 1985 Aug;42(2):177–81.

48. Laeger T, Henagan TM, Albarado DC, Redman LM, Bray GA, Noland RC, et al. FGF21 is an endocrine signal of protein restriction. J Clin Invest. 2014 Sept;124(9):3913–22.

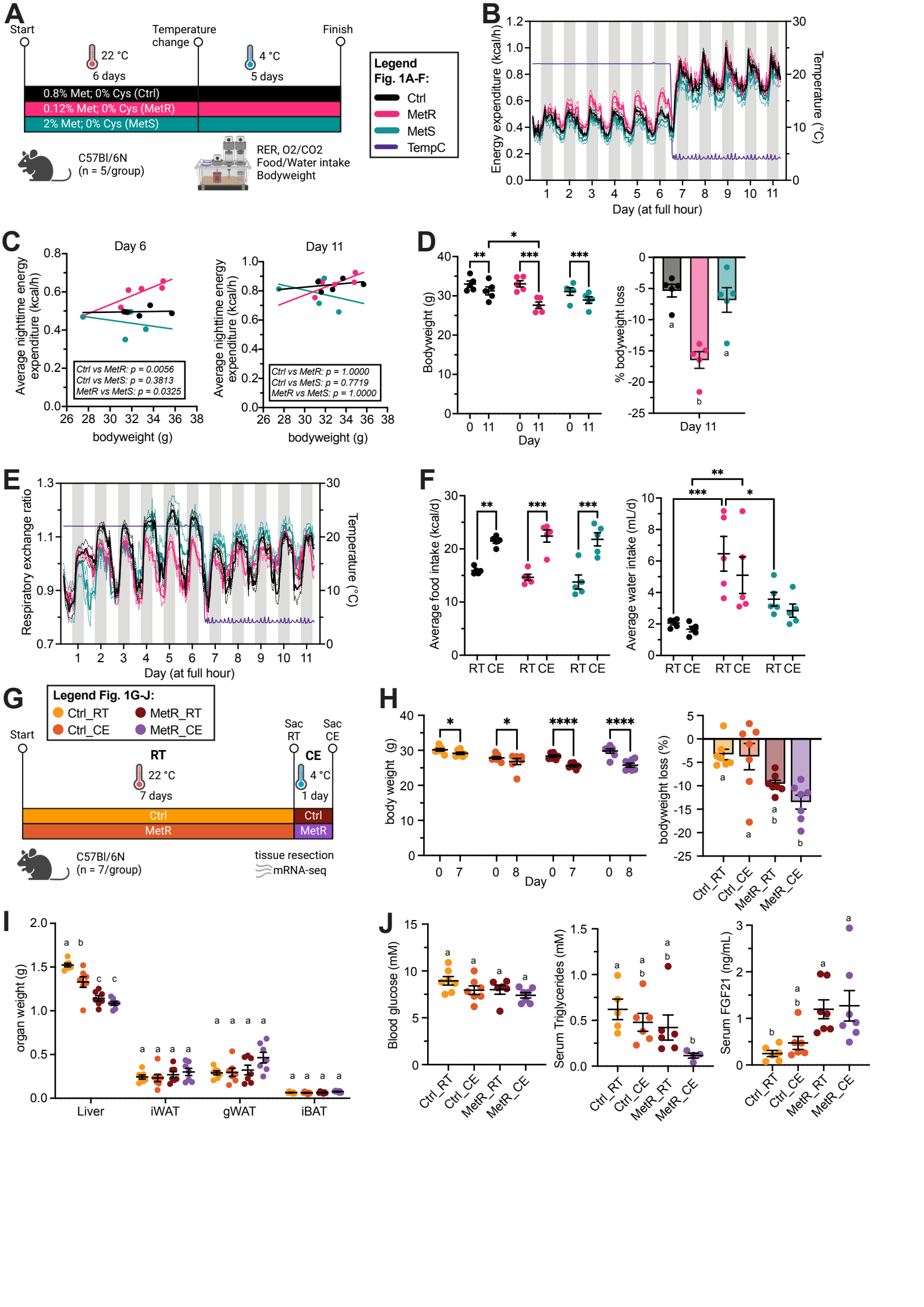
A
Start
Temperature change
Finish
22 °C
6 days
4 °C
5 days
0.8% Met; 0% Cys (Ctrl)
0.12% Met; 0% Cys (MetR)
2% Met; 0% Cys (MetS)
C57Bl/6N
(n = 5/group)
RER, O2/CO2
Food/Water intake
Bodyweight
Legend
Fig. 1A-F:
Ctrl
MetR
MetS
TempC
B
Energy expenditure (kcal/h)
Temperature (°C)
Day (at full hour)
C
Day 6
Day 11
Average nighttime energy expenditure (kcal/h)
bodyweight (g)
Ctrl vs MetR: p = 0.0056
Ctrl vs MetS: p = 0.3813
MetR vs MetS: p = 0.0325
Ctrl vs MetR: p = 1.0000
Ctrl vs MetS: p = 0.7719
MetR vs MetS: p = 1.0000
D
Bodyweight (g)
Day
% bodyweight loss
Day 11
E
Respiratory exchange ratio
Temperature (°C)
Day (at full hour)
F
Average food intake (kcal/d)
Average water intake (mL/d)
RT CE
G
Legend Fig. 1G-J:
Ctrl_RT
Ctrl_CE
MetR_RT
MetR_CE
Start
Sac RT
Sac CE
RT
22 °C
7 days
CE
4 °C
1 day
Ctrl
MetR
C57Bl/6N
(n = 7/group)
tissue resection
mRNA-seq
H
body weight (g)
Day
bodyweight loss (%)
I
organ weight (g)
Liver
iWAT
gWAT
iBAT
J
Blood glucose (mM)
Serum Triglycerides (mM)
Serum FGF21 (ng/mL)

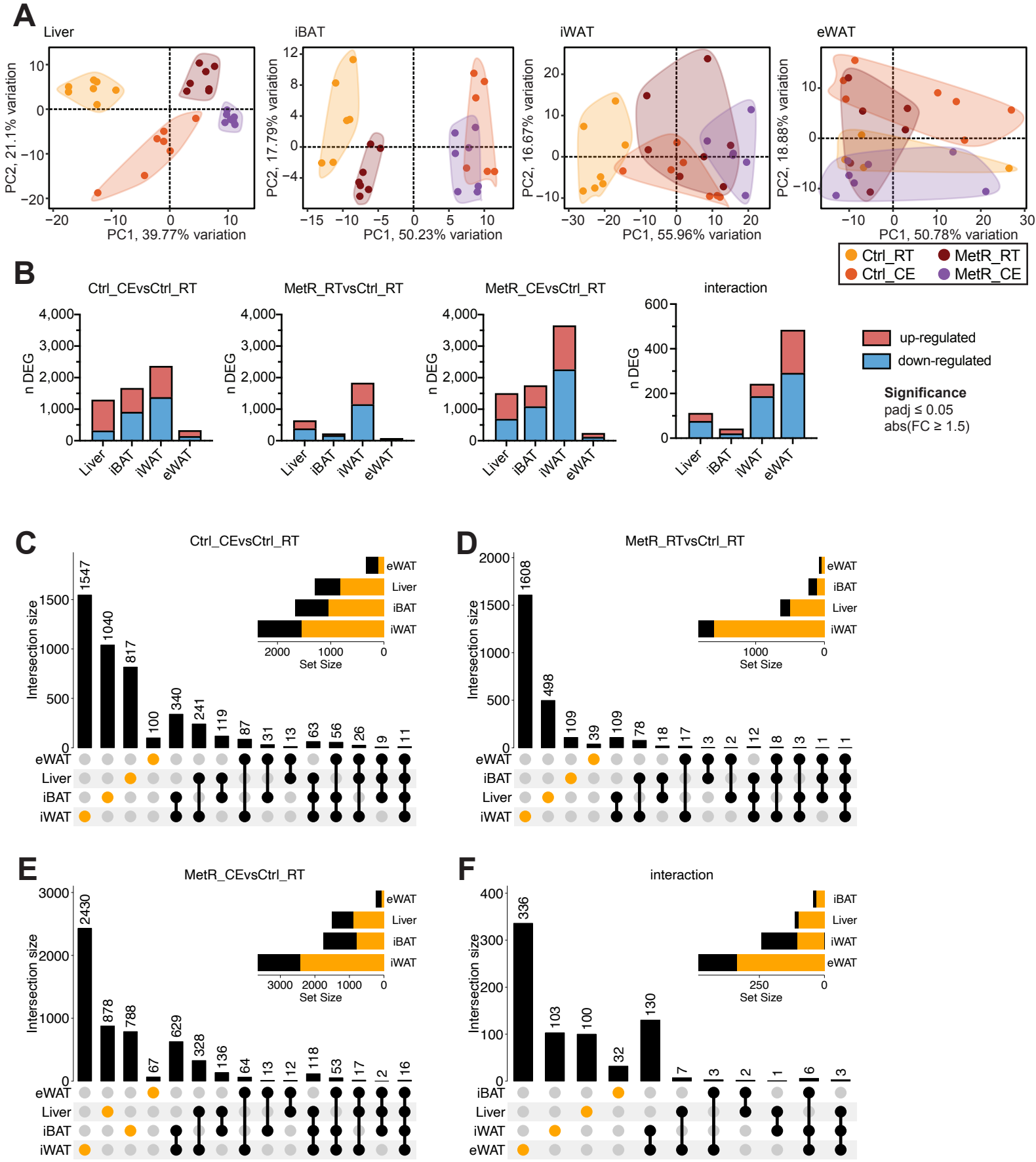
A
Liver
iBAT
iWAT
eWAT
PC2, 21.1% variation
PC1, 39.77% variation
PC2, 17.79% variation
PC1, 50.23% variation
PC2, 16.67% variation
PC1, 55.96% variation
PC2, 18.88% variation
PC1, 50.78% variation
Ctrl_RT
Ctrl_CE
MetR_RT
MetR_CE
B
Ctrl_CEvsCtrl_RT
MetR_RTvsCtrl_RT
MetR_CEvsCtrl_RT
interaction
n DEG
Liver
iBAT
iWAT
eWAT
up-regulated
down-regulated
Significance
padj ≤ 0.05
abs(FC ≥ 1.5)
C
Ctrl_CEvsCtrl_RT
Intersection size
Set Size
1547
1040
817
100
340
241
119
87
31
13
63
56
26
9
11
D
MetR_RTvsCtrl_RT
1608
498
109
39
109
78
18
17
3
2
12
8
3
1
1
E
MetR_CEvsCtrl_RT
2430
878
788
67
629
328
136
64
13
12
118
53
17
2
16
F
interaction
336
103
100
32
130
7
3
2
1
6
3

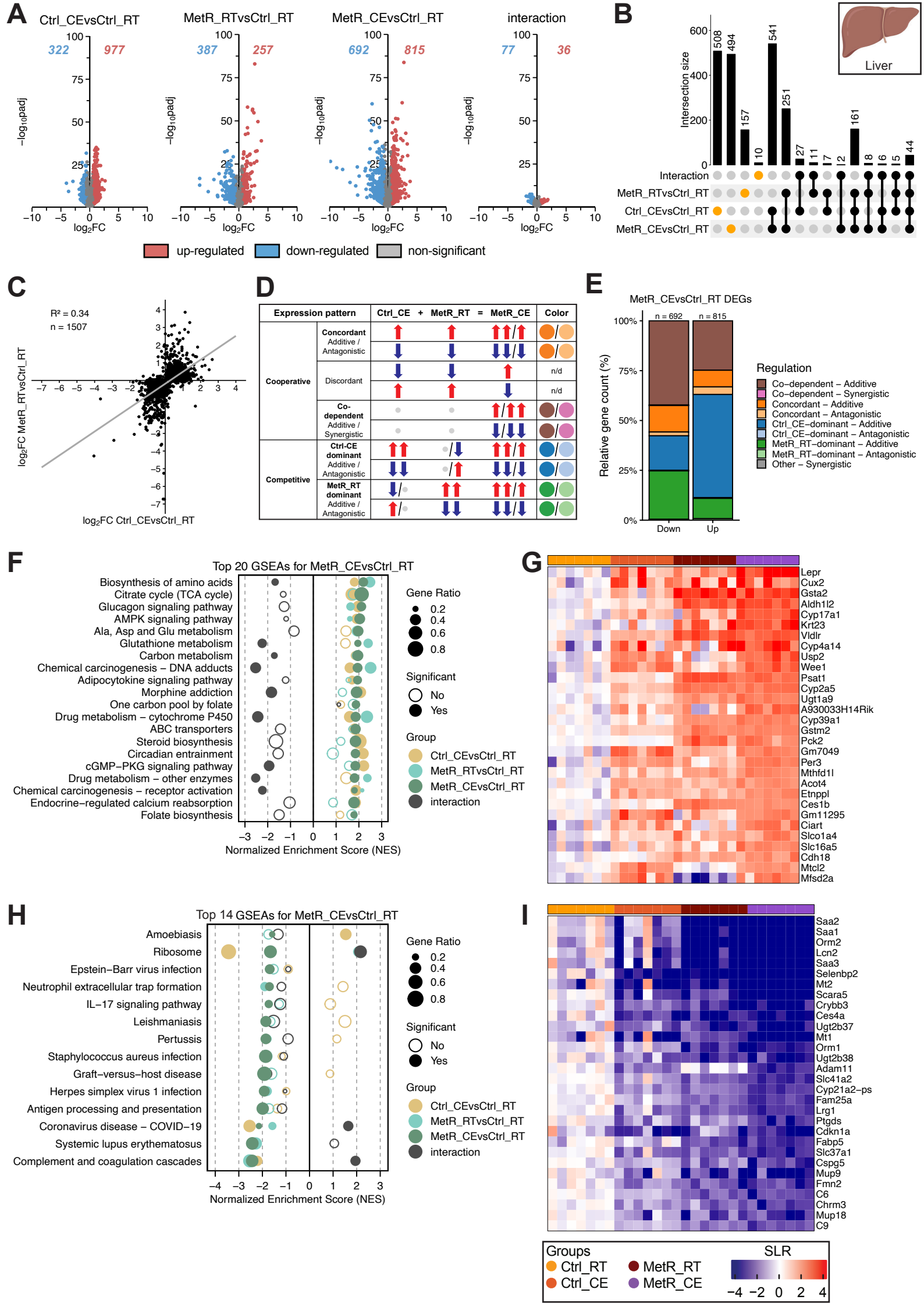
A
Ctrl_CEvsCtrl_RT
322
977
MetR_RTvsCtrl_RT
387
257
MetR_CEvsCtrl_RT
692
815
interaction
77
36
−log10padj
log2FC
up-regulated
down-regulated
non-significant
B
Liver
Intersection size
508
494
157
10
541
251
27
11
7
2
161
8
6
5
44
Interaction
MetR_RTvsCtrl_RT
Ctrl_CEvsCtrl_RT
MetR_CEvsCtrl_RT
C
R² = 0.34
n = 1507
log2FC MetR_RTvsCtrl_RT
log2FC Ctrl_CEvsCtrl_RT
D
Expression pattern
Ctrl_CE + MetR_RT = MetR_CE
Color
Cooperative
Concordant Additive / Antagonistic
Discordant
n/d
Co-dependent Additive / Synergistic
Competitive
Ctrl-CE dominant Additive / Antagonistic
MetR_RT dominant Additive / Antagonistic
E
MetR_CEvsCtrl_RT DEGs
n = 692
n = 815
Relative gene count (%)
Down
Up
Regulation
Co−dependent − Additive
Co−dependent − Synergistic
Concordant − Additive
Concordant − Antagonistic
Ctrl_CE−dominant − Additive
Ctrl_CE−dominant − Antagonistic
MetR_RT−dominant − Additive
MetR_RT−dominant − Antagonistic
Other − Synergistic
F
Top 20 GSEAs for MetR_CEvsCtrl_RT
Biosynthesis of amino acids
Citrate cycle (TCA cycle)
Glucagon signaling pathway
AMPK signaling pathway
Ala, Asp and Glu metabolism
Glutathione metabolism
Carbon metabolism
Chemical carcinogenesis − DNA adducts
Adipocytokine signaling pathway
Morphine addiction
One carbon pool by folate
Drug metabolism − cytochrome P450
ABC transporters
Steroid biosynthesis
Circadian entrainment
cGMP−PKG signaling pathway
Drug metabolism − other enzymes
Chemical carcinogenesis − receptor activation
Endocrine−regulated calcium reabsorption
Folate biosynthesis
Normalized Enrichment Score (NES)
Gene Ratio
Significant
No
Yes
Group
Ctrl_CEvsCtrl_RT
MetR_RTvsCtrl_RT
MetR_CEvsCtrl_RT
interaction
G
Lepr
Cux2
Gsta2
Aldh1l2
Cyp17a1
Krt23
Vldlr
Cyp4a14
Usp2
Wee1
Psat1
Cyp2a5
Ugt1a9
A930033H14Rik
Cyp39a1
Gstm2
Pck2
Gm7049
Per3
Mthfd1l
Acot4
Etnppl
Ces1b
Gm11295
Ciart
Slco1a4
Slc16a5
Cdh18
Mtcl2
Mfsd2a
H
Top 14 GSEAs for MetR_CEvsCtrl_RT
Amoebiasis
Ribosome
Epstein−Barr virus infection
Neutrophil extracellular trap formation
IL−17 signaling pathway
Leishmaniasis
Pertussis
Staphylococcus aureus infection
Graft−versus−host disease
Herpes simplex virus 1 infection
Antigen processing and presentation
Coronavirus disease − COVID−19
Systemic lupus erythematosus
Complement and coagulation cascades
Normalized Enrichment Score (NES)
Gene Ratio
Significant
No
Yes
Group
Ctrl_CEvsCtrl_RT
MetR_RTvsCtrl_RT
MetR_CEvsCtrl_RT
interaction
I
Saa2
Saa1
Orm2
Lcn2
Saa3
Selenbp2
Mt2
Scara5
Crybb3
Ces4a
Ugt2b37
Mt1
Orm1
Ugt2b38
Adam11
Slc41a2
Cyp21a2−ps
Fam25a
Lrg1
Ptgds
Cdkn1a
Fabp5
Slc37a1
Cspg5
Mup9
Fmn2
C6
Chrm3
Mup18
C9
Groups
Ctrl_RT
Ctrl_CE
MetR_RT
MetR_CE
SLR

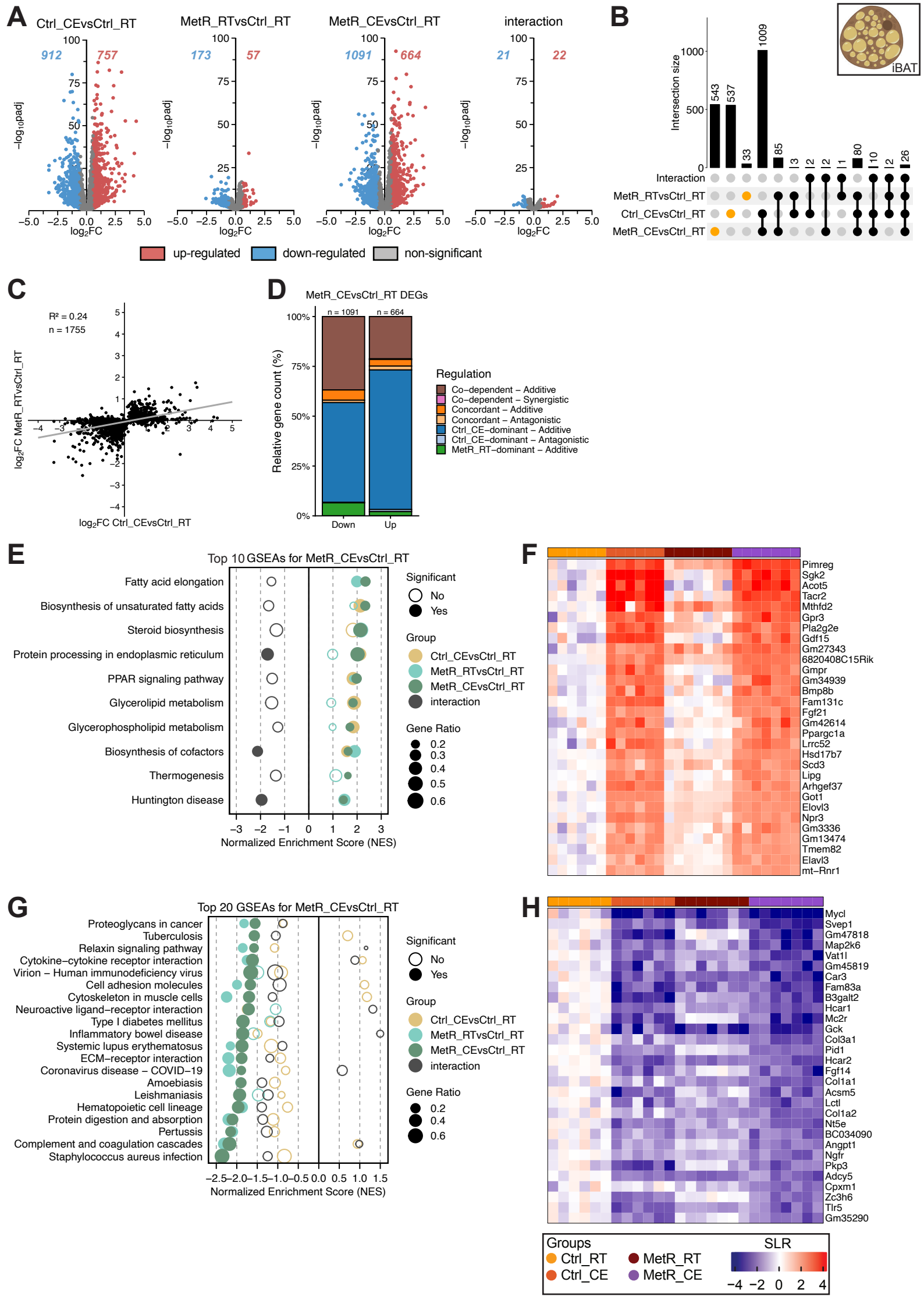
A
Ctrl_CEvsCtrl_RT
MetR_RTvsCtrl_RT
MetR_CEvsCtrl_RT
interaction
912
757
173
57
1091
664
21
22
−log10padj
log2FC
up-regulated
down-regulated
non-significant
B
iBAT
Intersection size
543
537
33
1009
85
3
2
2
1
80
10
2
26
Interaction
MetR_RTvsCtrl_RT
Ctrl_CEvsCtrl_RT
MetR_CEvsCtrl_RT
C
R² = 0.24
n = 1755
log2FC MetR_RTvsCtrl_RT
log2FC Ctrl_CEvsCtrl_RT
D
MetR_CEvsCtrl_RT DEGs
n = 1091
n = 664
Relative gene count (%)
Down
Up
Regulation
Co−dependent − Additive
Co−dependent − Synergistic
Concordant − Additive
Concordant − Antagonistic
Ctrl_CE−dominant − Additive
Ctrl_CE−dominant − Antagonistic
MetR_RT−dominant − Additive
E
Top 10 GSEAs for MetR_CEvsCtrl_RT
Fatty acid elongation
Biosynthesis of unsaturated fatty acids
Steroid biosynthesis
Protein processing in endoplasmic reticulum
PPAR signaling pathway
Glycerolipid metabolism
Glycerophospholipid metabolism
Biosynthesis of cofactors
Thermogenesis
Huntington disease
Normalized Enrichment Score (NES)
Significant
No
Yes
Group
Ctrl_CEvsCtrl_RT
MetR_RTvsCtrl_RT
MetR_CEvsCtrl_RT
interaction
Gene Ratio
F
Pimreg
Sgk2
Acot5
Tacr2
Mthfd2
Gpr3
Pla2g2e
Gdf15
Gm27343
6820408C15Rik
Gmpr
Gm34939
Bmp8b
Fam131c
Fgf21
Gm42614
Ppargc1a
Lrrc52
Hsd17b7
Scd3
Lipg
Arhgef37
Got1
Elovl3
Npr3
Gm3336
Gm13474
Tmem82
Elavl3
mt−Rnr1
G
Top 20 GSEAs for MetR_CEvsCtrl_RT
Proteoglycans in cancer
Tuberculosis
Relaxin signaling pathway
Cytokine−cytokine receptor interaction
Virion − Human immunodeficiency virus
Cell adhesion molecules
Cytoskeleton in muscle cells
Neuroactive ligand−receptor interaction
Type I diabetes mellitus
Inflammatory bowel disease
Systemic lupus erythematosus
ECM−receptor interaction
Coronavirus disease − COVID−19
Amoebiasis
Leishmaniasis
Hematopoietic cell lineage
Protein digestion and absorption
Pertussis
Complement and coagulation cascades
Staphylococcus aureus infection
Normalized Enrichment Score (NES)
Significant
No
Yes
Group
Ctrl_CEvsCtrl_RT
MetR_RTvsCtrl_RT
MetR_CEvsCtrl_RT
interaction
Gene Ratio
H
Mycl
Svep1
Gm47818
Map2k6
Vat1l
Gm45819
Car3
Fam83a
B3galt2
Hcar1
Mc2r
Gck
Col3a1
Pid1
Hcar2
Fgf14
Col1a1
Acsm5
Lctl
Col1a2
Nt5e
BC034090
Angpt1
Ngfr
Pkp3
Adcy5
Cpxm1
Zc3h6
Tlr5
Gm35290
Groups
Ctrl_RT
Ctrl_CE
MetR_RT
MetR_CE
SLR

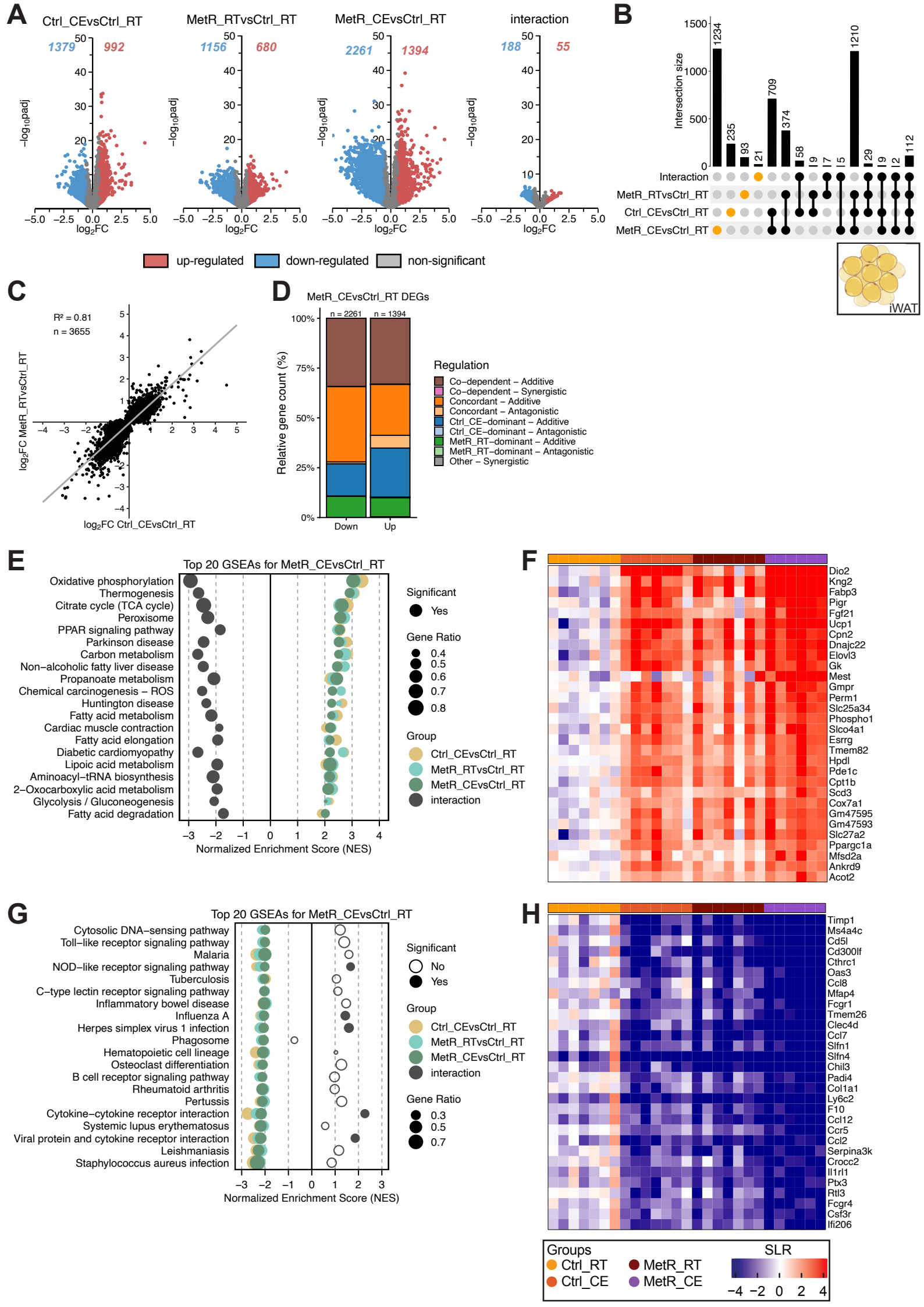
A
Ctrl_CEvsCtrl_RT
1379
992
MetR_RTvsCtrl_RT
1156
680
MetR_CEvsCtrl_RT
2261
1394
interaction
188
55
−log10padj
log2FC
up-regulated
down-regulated
non-significant
B
Intersection size
1234
235
93
21
709
374
58
19
17
15
1210
29
19
12
112
Interaction
MetR_RTvsCtrl_RT
Ctrl_CEvsCtrl_RT
MetR_CEvsCtrl_RT
iWAT
C
R² = 0.81
n = 3655
log2FC MetR_RTvsCtrl_RT
log2FC Ctrl_CEvsCtrl_RT
D
MetR_CEvsCtrl_RT DEGs
n = 2261
n = 1394
Relative gene count (%)
Down
Up
Regulation
Co−dependent − Additive
Co−dependent − Synergistic
Concordant − Additive
Concordant − Antagonistic
Ctrl_CE−dominant − Additive
Ctrl_CE−dominant − Antagonistic
MetR_RT−dominant − Additive
MetR_RT−dominant − Antagonistic
Other − Synergistic
E
Top 20 GSEAs for MetR_CEvsCtrl_RT
Oxidative phosphorylation
Thermogenesis
Citrate cycle (TCA cycle)
Peroxisome
PPAR signaling pathway
Parkinson disease
Carbon metabolism
Non−alcoholic fatty liver disease
Propanoate metabolism
Chemical carcinogenesis − ROS
Huntington disease
Fatty acid metabolism
Cardiac muscle contraction
Fatty acid elongation
Diabetic cardiomyopathy
Lipoic acid metabolism
Aminoacyl−tRNA biosynthesis
2−Oxocarboxylic acid metabolism
Glycolysis / Gluconeogenesis
Fatty acid degradation
Normalized Enrichment Score (NES)
Significant
Yes
Gene Ratio
0.4
0.5
0.6
0.7
0.8
Group
Ctrl_CEvsCtrl_RT
MetR_RTvsCtrl_RT
MetR_CEvsCtrl_RT
interaction
F
Dio2
Kng2
Fabp3
Pigr
Fgf21
Ucp1
Cpn2
Dnajc22
Elovl3
Gk
Mest
Gmpr
Perm1
Slc25a34
Phospho1
Slco4a1
Esrrg
Tmem82
Hpdl
Pde1c
Cpt1b
Scd3
Cox7a1
Gm47595
Gm47593
Slc27a2
Ppargc1a
Mfsd2a
Ankrd9
Acot2
G
Top 20 GSEAs for MetR_CEvsCtrl_RT
Cytosolic DNA−sensing pathway
Toll−like receptor signaling pathway
Malaria
NOD−like receptor signaling pathway
Tuberculosis
C−type lectin receptor signaling pathway
Inflammatory bowel disease
Influenza A
Herpes simplex virus 1 infection
Phagosome
Hematopoietic cell lineage
Osteoclast differentiation
B cell receptor signaling pathway
Rheumatoid arthritis
Pertussis
Cytokine−cytokine receptor interaction
Systemic lupus erythematosus
Viral protein and cytokine receptor interaction
Leishmaniasis
Staphylococcus aureus infection
Normalized Enrichment Score (NES)
Significant
No
Yes
Group
Ctrl_CEvsCtrl_RT
MetR_RTvsCtrl_RT
MetR_CEvsCtrl_RT
interaction
Gene Ratio
0.3
0.5
0.7
H
Timp1
Ms4a4c
Cd5l
Cd300lf
Cthrc1
Oas3
Ccl8
Mfap4
Fcgr1
Tmem26
Clec4d
Ccl7
Slfn1
Slfn4
Chil3
Padi4
Col1a1
Ly6c2
F10
Ccl12
Ccr5
Ccl2
Serpina3k
Crocc2
Il1rl1
Ptx3
Rtl3
Fcgr4
Csf3r
Ifi206
Groups
Ctrl_RT
Ctrl_CE
MetR_RT
MetR_CE
SLR

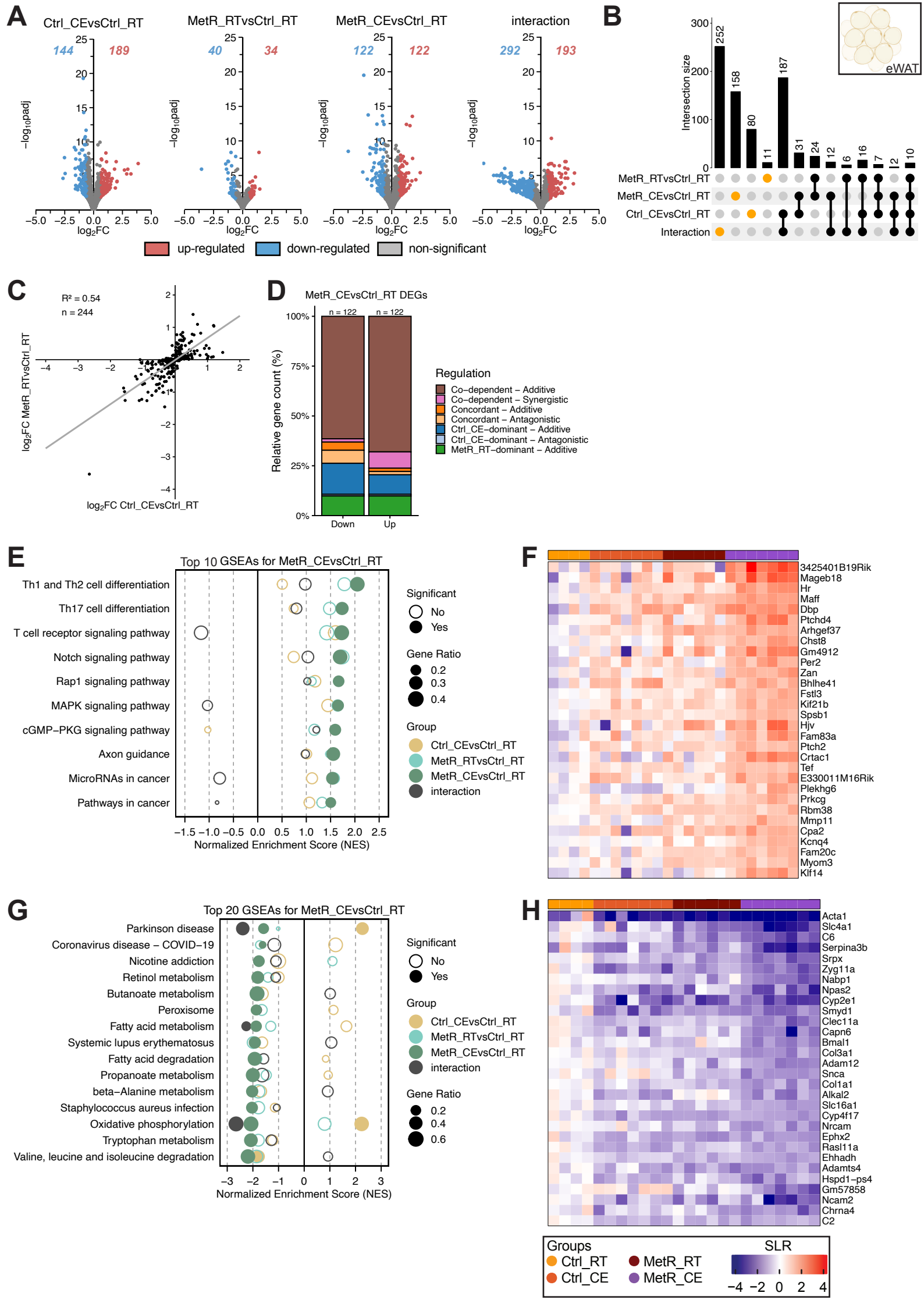
A
Ctrl_CEvsCtrl_RT
144
189
MetR_RTvsCtrl_RT
40
34
MetR_CEvsCtrl_RT
122
122
interaction
292
193
−log10padj
log2FC
up-regulated
down-regulated
non-significant
B
eWAT
Intersection size
252
158
80
11
187
31
24
12
6
16
7
2
10
MetR_RTvsCtrl_RT
MetR_CEvsCtrl_RT
Ctrl_CEvsCtrl_RT
Interaction
C
R² = 0.54
n = 244
log2FC MetR_RTvsCtrl_RT
log2FC Ctrl_CEvsCtrl_RT
D
MetR_CEvsCtrl_RT DEGs
n = 122
n = 122
Relative gene count (%)
Down
Up
Regulation
Co−dependent − Additive
Co−dependent − Synergistic
Concordant − Additive
Concordant − Antagonistic
Ctrl_CE−dominant − Additive
Ctrl_CE−dominant − Antagonistic
MetR_RT−dominant − Additive
E
Top 10 GSEAs for MetR_CEvsCtrl_RT
Th1 and Th2 cell differentiation
Th17 cell differentiation
T cell receptor signaling pathway
Notch signaling pathway
Rap1 signaling pathway
MAPK signaling pathway
cGMP−PKG signaling pathway
Axon guidance
MicroRNAs in cancer
Pathways in cancer
Normalized Enrichment Score (NES)
Significant
No
Yes
Gene Ratio
0.2
0.3
0.4
Group
Ctrl_CEvsCtrl_RT
MetR_RTvsCtrl_RT
MetR_CEvsCtrl_RT
interaction
F
3425401B19Rik
Mageb18
Hr
Maff
Dbp
Ptchd4
Arhgef37
Chst8
Gm4912
Per2
Zan
Bhlhe41
Fstl3
Kif21b
Spsb1
Hjv
Fam83a
Ptch2
Crtac1
Tef
E330011M16Rik
Plekhg6
Prkcg
Rbm38
Mmp11
Cpa2
Kcnq4
Fam20c
Myom3
Klf14
G
Top 20 GSEAs for MetR_CEvsCtrl_RT
Parkinson disease
Coronavirus disease − COVID−19
Nicotine addiction
Retinol metabolism
Butanoate metabolism
Peroxisome
Fatty acid metabolism
Systemic lupus erythematosus
Fatty acid degradation
Propanoate metabolism
beta−Alanine metabolism
Staphylococcus aureus infection
Oxidative phosphorylation
Tryptophan metabolism
Valine, leucine and isoleucine degradation
Normalized Enrichment Score (NES)
Significant
No
Yes
Group
Ctrl_CEvsCtrl_RT
MetR_RTvsCtrl_RT
MetR_CEvsCtrl_RT
interaction
Gene Ratio
0.2
0.4
0.6
H
Acta1
Slc4a1
C6
Serpina3b
Srpx
Zyg11a
Nabp1
Npas2
Cyp2e1
Smyd1
Clec11a
Capn6
Bmal1
Col3a1
Adam12
Snca
Col1a1
Alkal2
Slc16a1
Cyp4f17
Nrcam
Ephx2
Rasl11a
Ehhadh
Adamts4
Hspd1−ps4
Gm57858
Ncam2
Chrna4
C2
Groups
Ctrl_RT
Ctrl_CE
MetR_RT
MetR_CE
SLR